Title
Diffusion-Controlled Evaporating Completely Wetting Meniscus in a Channel

Author
Njante, Jean-Pierre

Publication Date
2012

Peer reviewed|Thesis/dissertation

Diffusion-Controlled Evaporating Completely Wetting Meniscus in a Channel

By

Njante Jean-Pierre Nchuiwo

A dissertation submitted in partial satisfaction of the
requirements for the degree of
Doctor of Philosophy
in
Engineering–Mechanical Engineering
in the
Graduate Division
of the
University of California, Berkeley

Committee in charge:

Professor Stephen Morris, Chair
Professor Van P. Carey
Professor Clayton Radke

Spring 2012

Abstract

Diffusion-Controlled Evaporating Completely Wetting Meniscus in a Channel

by

Njante Jean-Pierre Nchuiwo

Doctor of Philosophy in Engineering
University of California, Berkeley
Professor Stephen Morris, Chair

We consider the evaporating meniscus of a perfectly wetting isochemical liquid formed in the gap between two horizontal flat plates. The plates are initially at common temperature with the surroundings, and liquid evaporates into a binary mixture of its own vapour and an inert component. The liquid evaporates because the partial pressure of the vapour decreases from its saturation value p_s at the bulk meniscus to ϕp_s at the channel mouth. Evaporation draws liquid into the contact region. Near the wetted walls, the resulting pressure differences distort the phase interface, creating an apparent contact angle Θ. To keep the interface stationary, liquid is continuously fed into the channel at the same rate $2\dot{m}$ as it is being evaporated.

To determine both Θ and $\dot{m}$, we make the following simplifying assumptions. (a) Liquid and vapour at the interface are in local thermodynamic equilibrium; as a result, evaporation is limited by diffusion of vapour molecules in the surrounding gas. (b) Evaporation is sufficiently slow that the system is effectively isothermal; though evaporation induces liquid temperature differences, they are kinetically negligible. Given (a) and (b), the vapour partial pressure is related to the liquid pressure by the Kelvin equation. Because the system is completely wetting, the visible meniscus is preceded by a thin wetting film; we assume that the channel gap thickness $2a$ is significantly large compared with the hydrostatic solution for the wetting film thickness. This disparity in length scales gives the theory an inner and outer structure. Within the small scale inner region, the lubrication approximation holds, and diffusion in the gas is one-dimensional along the axis. As a result, the inner problem is reduced to a pair of second order nonlinear ordinary differential equations for the liquid pressure and interface shape. Because the capillary

number, based on the velocity of the induced flow, is assumed negligible, the large scale outer region is approximated by a circular arc meniscus.

We analyse the inner problem numerically using the spline collocation method. Though the hydrostatic contact angle is zero for a completely wetting system, Θ is found to be an increasing function of the imposed pressure difference $p_s(1-\phi)$. We derive a formula for Θ as a function of material properties and $p_s(1-\phi)$. Though microphysics must be included in the inner problem to resolve a singularity in the hydrodynamic equations, Θ is insensitive to the microphysical details. Our analysis shows that Θ is determined chiefly by a capillary number $Ca = \mu_\ell V_s/\gamma$ based on surface tension γ, liquid viscosity μ_ℓ, and a velocity scale V_s for liquid flow set by evaporation.

Because the vapour pressure above the outer circular arc meniscus is uniform, the total evaporation from the capillary is determined within the inner region. Our analysis shows that because the Stefan diffusion theory, described by Bird et al (2006, pg 545)[43], does not account for mass loss from the thin precursor film, it significantly under-estimates the total evaporation from small (typically μm-sized) capillaries. Even though the simplified analysis by Derjaguin et al[1] describes only film thicknesses less than the precursor film thickness for hydrostatic equilibrium, we find that their simplified equations correctly determines the total evaporation from capillaries if the length of the gas column L is large compared with the channel gap thickness $2a$.

Contents

Chapter 1

Introduction

Temperature control by evaporation of completely wetting liquids is of critical importance to many heat transfer processes and devices ranging from micro heat pipes to grooved evaporators. In these examples, evaporation is driven by an imposed heat flux. This thesis focuses on the opposite situation where there is no applied wall superheat; the drop and surroundings are initially at the same temperature, and the pure liquid evaporates into a binary mixture of its own vapour and an inert component in response to a concentration gradient of the vapour molecules in the gas. Recent interest in this field has been aroused by the so called coffee-stain problem. As observed by Deegan et al (2000, fig 1)[19], a drop of coffee left to dry on a counter-top leaves a ring, rather than a uniform spot, of solute deposits. Given that the coffee solute was uniformly distributed in the liquid prior to drying, its segregation to the drop edge is intriguing. Ring deposits are commonly observed when drops containing dispersed particles evaporate on cool surfaces; everyday examples include mineral rings left on washed glassware, banded deposits of salt on the side-walk during winter, and enhanced edges in water colour paintings.

Understanding evaporation-driven deposition is critical to many industrial processes and devices. In ink-jet printing, for instance, the liquid beads are deposited on a substrate and attempts are made to control segregation by controlling the evaporation profile of the drying beads[4]. Paint manufactures use various additives to ensure that the pigments remain evenly dispersed during and after drying. While segregation effects are undesirable in the above examples, they could become indispensable for other processes such as in DNA patterning for gene expression analysis[5], production of nano-fibres using dry spinning techniques[6], and in drop coating deposition Raman

method for drug discovery[7]. It is therefore obvious that a thorough understanding of the segregation process is of critical importance, especially to those practitioners who must enhanced[5−7] or eliminate[4] the process.

Despite its apparent simplicity, modelling evaporation near three-phase contact lines involves evaporation kinetics coupled with momentum, mass, and energy transfer between the phases. It is this coupling of the different physics between the phases that complicates the analysis; in effect, even when transport processes in the solid phase are not considered, the reduced set of governing equations are still of significant complexity[8,9]. The problem is further complicated because the free interface location is not known a priori, and so is obtained as part of the solution to the free boundary problem.

The degree of complexity is reduced by making the following simplifying assumptions: (*i*) The thermal conductivity of the liquid is significantly small compared with that of the solid; this allows us to neglect temperature differences within the solid phase, and to take the wall temperature as uniform, and because the liquid does not penetrate the wall, transport processes in the solid phase are not considered. (*ii*) The gas thermal conductivity, density, and viscosity are small compared with those of the liquid; however, the gas-liquid density ratio is retained in the interface mass balance relation because it multiplies the gas velocity, which may be large relative to the liquid velocity. Condition (*ii*) ensures that the momentum and energy equations for the gas are not considered. Therefore given (*i*) and (*ii*), evaporation near three-phase contact lines can be described by a system of differential equations consisting of the Navier-Stokes and energy equations in the liquid phase and the diffusion equation for the vapour in the gas phase; these equations are coupled through boundary conditions at the interface, and are further simplified by exploiting the disparity in length scales associated with thin film flows. For vanishingly small contact angles, the lateral length scales are much larger than the vertical ones, giving rise to small aspect ratios; this, in turn, opens the door to lubrication approximation. Numerical solutions[25] of the Stokes equations shows that the lubrication approximation is applicable even for contact angles as large as 40°. For the sufficiently slow evaporation processes considered in this analysis, convective non-linearities are negligibly small and the contact angles are usually less than 5°, making the lubrication approximation appropriate. Since the flow is approximately two-dimensional near the drop edge, Oron et al[38] integrated the liquid equations, written in the lubrication limit, to show that the drop profile h satisfies,

$$\rho_\ell \frac{\partial h}{\partial t} + \frac{\partial}{\partial x}\left[\frac{h^3}{3\nu}\frac{\partial}{\partial x}\left(\gamma\frac{\partial^2 h}{\partial x^2} + \frac{A}{h^3}\right) + \frac{h^2}{2\nu}\frac{\partial \gamma}{\partial x}\right] = -J \tag{1.1}$$

where A is the dispersion constant, γ the surface tension, ν the liquid kinematic viscosity, ρ_ℓ the liquid density, $J(x,t)$ the evaporative mass flux normal to the interface, x the wall coordinate, and t the time variable.

1.1 Existing theories used to Predict J

Cazabat and Guena[12] have recently reviewed these theories. Transport processes in the liquid are coupled to those in the gas through J. This coupling of the different physics between the phases complicates the analysis; it is for this reason that researchers in this field have resorted to approximations that have ended up splitting the literature into two different bodies. In either body of research, the evaporative flux is computed by ignoring the dynamics in one of the phases; which phase to ignore depends on the boundary condition driving evaporation in the first place. In the thermal model, a heat flux is imposed, and evaporation is assumed to be controlled by heat conduction in the liquid layer; in the Langmuir diffusion model, a concentration gradient is imposed in the gas phase, and stationary diffusion of the vapour molecules in the gas is assumed to be the limiting mechanism for the evaporation rate.

1.1.1 The Langmuir Diffusion Theory

The evaporation of isolated spherical droplets in quiescent atmosphere has been studied by Morse[2]. The mm-sized spheres were placed in a microbalance and weighed at intervals until they disappeared. The experiments indicated that the rate of mass loss was proportional to the radius of the sphere and not to its surface. This result is surprising. Due to spherical symmetry, the local evaporative flux is uniform at the drop surface, and one would have expected the total evaporation rate to scale with the drop area. Langmuir[3] explained Morse's result by first assuming that the gas just above the drop surface is saturated with the liquid's vapour, and that evaporation is controlled by stationary diffusion of the vapour molecules in the surrounding gas. He then posed the following boundary value problem for the vapour density ρ_v,

$$\bigtriangledown^2\rho_v(r) = 0; \quad \rho_v(R) = \rho_{sat}, \quad \rho_v(\infty) = \phi\rho_{sat}, \quad J = -D_v\rho_v'(R) \quad \text{(1.2a-d)}$$

where R is the drop radius, D_v the binary diffusion coefficient, ρ_v' differentiation with respect to the radial coordinates r. The vapour density ρ_v is given in units of kg/m^3. Because the liquid evaporates into a mixture, the vapour concentration is non-uniform above the drop. At the drop surface, the vapour concentration is fixed at its saturation value ρ_{sat} at system temperature. Far from the drop surface, $\rho_v = \phi\rho_{sat}$, where ϕ is the relative humidity in the distant gas. The concentration difference $\Delta\rho = \rho_{sat}(1-\phi)$ drives evaporation in accordance with the diffusion equation (1.2a). Langmuir integrated this equation to show that $M'(t) = -4\pi R D_v \Delta\rho$, which is in agreement with Morse's observation. Here, $M(t)$ is the drop mass at time t. Because the drop volume scales like R^3, its radius scales like $\sqrt{t_f - t}$, where t_f is the time it takes the drop to disappear. The evaporative flux $J = D_v\Delta\rho/R$.

In what follows, we use evaporation from sessile droplets as example of a flow in which evaporation is diffusion controlled, and for which contact angles have been observed and measured by Benichou et al (2003, fig 14)[16]. Now a substrate comes into play, and the wetted area is limited by a contact line. The only modification to problem (1.2) is to impose a zero flux ahead of the contact line; this assumes that the system is partially wetting, and that the vapour does not penetrate the wall. Picknett and Bexon[21] find J by solving an equivalent electrostatic problem, in which ρ_v is the electrostatic potential and the drop surface a conductor at fixed potential. For small contact angles, the electrostatic equivalence is a flat disc, for which solutions are given by

$$\frac{dM}{dt} = -4D_v R\Delta\rho, \qquad J = \frac{2D_v\Delta\rho}{\pi\sqrt{R^2 - r^2}}, \qquad M = \rho_\ell\frac{\pi\theta}{4}R^3 \qquad \text{(1.3a-c)}$$

The evaporative flux J diverges at the contact line $r = R$. Deegan et al[18] used this divergence to explain ring formation, in which the coffee flows towards the fixed contact line in order to replenish mass lost from evaporation, and once there, the solvent evaporates leaving the solutes to form the stain. For pinned contact lines, say due to surface inhomogeneity or dispersed particles in the liquid, equations (1.3a,c) predict that the contact angle and drop mass each scales like $(t_f - t)$, where t_f is the time it takes the drop to disappear.

This prediction is observed in experiments[21,18] on partially wetting system.

In the Picknett and Bexon solution, it is assumed that the drop maintains a spherical cap during the drying process; this requires two things. First, the drop radius must be small compared with the capillary length so that surface tension, which tends to make drops spherical, is large compared with gravitational forces, which tend to flatten the drops. Secondly, the evaporative induced liquid flow must be very weak so that the drop shape is not altered by the liquid motion. This second point is questionable near the leading edge of the drop, where evaporation is strongest. Physically, liquid flows from the bulk meniscus into the contact region in order to compensate for evaporation. Near the drop edge where evaporation is strongest, the flow becomes strong enough to distort the interface and creates a contact angle. Therefore, the spherical cap assumption must be reconsidered near the leading edge of the drop, where the flow can no longer be separated from the drop shape.

The diffusion process is quasi-stationary if the time taken for the drop to dry is significantly larger than the time $t_d = R^2/D_v$ required for a vapour molecule to travel a distance of order R. For a millimetre-sized water droplet evaporating in still air, the diffusion time scale $t_d \sim 0.1s$, which is far less than the time taken for a water drop to dry. The same conclusion is reached with the alkanes. The assumption of a quasi-stationary diffusion process is therefore valid in usual cases. We have assumed that evaporation is sufficiently slow that fluid inertia is everywhere negligible. Experiment using hanging drops of alkanes and water shows that unless there is an imposed air draft, convection in the gas has negligible effects on the evaporation rate[17].

Picknett and Bexon assumed that the system is effectively isothermal, even though the latent heat consumption caused by evaporation at the interface induces temperature gradients in the drop, substrate, and surrounding gas. Because the gas thermal conductivity is generally small compared with that of the drop, thermal exchanges with the gas phase are usually ignored, and only the drop and substrate are considered when writing the energy balance. The simple case is when the thermal conductivity of the substrate is large compared with that of the drop, so that thermal gradients in the substrate are negligible. Then the substrate temperature is uniform, equalling that in the distant gas, and the local temperature along the drop surface can be computed using the energy equation in the liquid. An order of magnitude analysis, see table A.1 in appendix A.2, shows that temperature differences across the drop are negligible for thin drops. This scaling law is consistent with numerical solutions by Hu et al[24]. The assumption of isothermal evap-

oration therefore holds for drops with small contact angles. For thick drops, temperature differences can be huge, and the resulting gradients in surface tension can significantly modify the hydrodynamic flow in the drop[24].

In the Picknett and Bexon solution, it is assumed that liquid and vapour at the interface are in thermodynamic equilibrium at wall temperature; this requires that the rate of transfer of molecules across the interface be fast so that diffusion of the vapour molecules in the gas becomes the rate-limiting step controlling the evaporation rate. This condition is met if the drop radius is large compared with the mean free path Λ of the vapour molecules in the surrounding gas. For small drops, the evaporation rate is no longer controlled by stationary diffusion, but by the rate of transfer of molecules across the interface. The recent theory by Sultan et al[11] for thin films accounts for both transfer of molecules across the interface and stationary diffusion in the gas phase, where it is reported that the rate of transfer of molecules across the interface becomes the rate-limiting step controlling the evaporation rate once the film thickness becomes small compared to Λ; otherwise, diffusion controls the evaporation rate. For most liquids in practice, $\Lambda \sim 0.1\mu m$.

A macroscopic drop on a surface is surrounded by a thin precursor film, typically a few tens of nanometres thick. In the Picknett solution, it is assumed that evaporation from the precursor film is negligible. However, the recent experiments by Benichou et al (2003, figs 12,13)[16] not only observe a film growing ahead of the contact line, but also observe significant evaporation from the precursor film. It is only recently that the completely wetting system has been studied in the literature, noticeably by Cazabat et al[12–17]. Now, the contact line moves freely through the whole drop life, and there is no pinning. As shown in Cazabat et al (2010, fig 8)[12], the drop first spreads because the liquid is wetting, the radius reaches a maximum value where it stays approximately constant for some time, and then recedes because of evaporation. Benichou et al (2003, fig 14)[16] have observed and measured contact angles for completely wetting evaporating droplets. If evaporation is controlled by stationary diffusion, then the Langmuir diffusion theory predicts that the radius $R \propto (t_f - t)^{1/2}$. This prediction has been compared with experimental data; Cazabat et al (2010, table 2)[12] fitted the data to the power law behaviour $R \propto (t_f - t)^y$, and measured values for y that are indeed close to 0.5. In contrast, the power law $\theta \propto (t_f - t)^x$ is not well obeyed for the contact angle. Poulard et al[15] concluded that whereas the dynamics of the drop radius is well described by the Langmuir diffusion theory, the contact angle is very sensitive to all of the parameters involved.

1.1.2 The Thermal Model

All the work discussed so far are based on the assumption that the sessile drop and its surroundings were initially at the same temperature; temperature gradients, if any, are due solely to the drop's own evaporation. There is another body of research which concentrates on cases where the substrate is slightly superheated. In this case, the interface is not at thermodynamic equilibrium, and evaporation is controlled by the rate of transfer of molecules across the interface. The simplest case is when the liquid evaporates into its own vapour. Then the dynamical processes in the gas phase are ignored for the purpose of computing the evaporation rate. This approach has extensively been used to describe stationary meniscus of completely wetting isochemical liquid evaporating into its own vapour (Wayner et al[26–31], Moosman and Homsy[32], Morris[35–37]). The evaporation rate is determined by heat conduction in the liquid film, and is given by the Herz-Knudsen equation, see equation (11) in Camenga[42]. The controlling parameter is the applied wall superheat, and the apparent contact angle is an increasing function of superheat. See Oron et al[38] for a comprehensive review of the thermal model.

1.2 Evaporation from capillaries

In the model of the Stefan diffusion tube described by Bird et al. (2006, pg 545)[43], the concentration field is assumed to be one–dimensional. However, as we now argue, local analysis of the contact region implies that for a wetting system (contact angle $< \pi/2$), this picture is incomplete, even before we consider the effect of the precursor film.

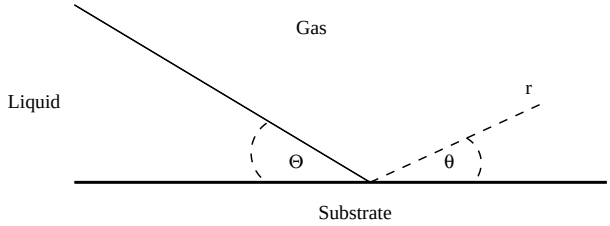

Figure 1.1: Contact Region

Figure 1.1 shows the geometry of the contact region: the contact angle measured through the liquid is denoted by Θ, (r, θ) are polar coordinates

with $\theta = 0$ on the substrate–gas interface. As formulated by Deegan et al.[18], near the contact line the vapour density ρ_v satisfies the following boundary value problem: for $0 < \theta < \pi - \Theta$

$$\nabla^2 \rho_v(r, \theta) = 0 \qquad \text{within the gas} \tag{1.4a}$$

$$at \quad \theta = 0, \qquad \frac{\partial \rho_v}{\partial \theta} = 0 \tag{1.4b}$$

$$at \quad \theta = \pi - \Theta, \qquad \rho_v = \rho_{sat} \tag{1.4c}$$

As discussed by Jackson (1975,p.77)[46], separation of variables can be used to determined a basis of solutions for this problem; only members of that basis for which the corresponding flux is integrable at $r = 0$ are physically pertinent. The dominant eigenfunction satisfying this condition is

$$\rho_v - \rho_{\rm sat} = r^n \cos n\theta, \qquad n = 1/(2 - 2\Theta/\pi). \tag{1.5a,b}$$

In the discussion in Bird et al. (2006, pg 545)[43], it is implicitly assumed that the contact angle $\Theta = \pi/2$. According to equation (1.5), in that case, $n = 1$; because the corresponding gradient is finite at $r = 0$, there is no possibility for concentration of evaporation near the contact line. This prediction of a local analysis is, of course, consistent with the solution of the boundary value problem describing the concentration field ρ_v throughout the entire Stefan diffusion tube: that boundary value problem admits a one–dimensional solution in which ρ_v depends only on distance x from the interface.

For $\Theta < \pi/2$, the phase interface is curved, and the boundary value problem for the entire tube no longer admits a one–dimensional solution. According to (1.5b), $n < 1$; because the corresponding gradient is singular at $r = 0$, local analysis allows the possibility that for a wetting system, evaporation is concentrated near the apparent contact line. For a sessile liquid droplet evaporating from a substrate on which the contact angle is less than $\pi/2$, Deegan et al. (1999, Fig.13)[19] show that the flux is indeed singular at the contact line, in quantitative agreement with the local analysis.

Though not accounting for the precursor film, the Deegan et al. analysis shows that for wetting systems evaporation is concentrated in the contact region. We might expect that for completely wetting systems, those for which the spreading coefficient is positive, the precursor film existing ahead of the

apparent contact line will also contribute to the total evaporation. This possibility is considered by Derjaguin et al.[1]; they conclude that the precursor film can contribute significantly to the mass transport near the state of hydrostatic equilibrium if the evaporation is weak. Though we confirm this conclusion, we are chiefly interesting in the Derjaguin limiting case as check on our numerical work.

1.3 Scope and Outline of Thesis

In the drop geometry, one will have to match a two dimensional flow near the drop edge to a three dimensional flow in the distant gas. This matching is extremely difficult and un-necessary since we are only interested in the dynamical processes near the contact line. For this reason, we study the corresponding problem for the channel geometry, where the outer flow is simplified. The channel geometry has been used by Derjaguin et al[1] to study evaporation from small (μm-sized) tubes. They find, both theoretically and experimentally, that as the tube diameter is reduced, the Stefan diffusion theory significantly under-estimates the total evaporation from capillaries; they explained the discrepancy by accounting for evaporation from the thin precursor film. Derjaguin et al simplified the description of the bulk meniscus in a way that does not allow for the existence of a contact angle; our work is an advance over their analysis because including surface tension γ allows us to calculate the shape of the whole meniscus and to predict contact angles.

Because the system is completely wetting, the seemingly un-wetted walls are actually covered with a thin wetting film. We assume that the thickness of that wetting film is significantly small compared with the channel gap thickness. In chapter 2, we simplify the analysis by taking advantage of the disparity in length scales to separate the meniscus into an inner and outer structure. Within the large scale outer region II, the interface is approximated by a circular arc because for vanishing capillary number, the induced flow is too weak to alter the shape of the bulk meniscus. Within the small scale inner region I, the induced flow is strong enough to perturb the interface so that the pressure fields on both sides of the interface, together with the interface shape are described by a free boundary problem coupling wetting physics to evaporation kinetics, lubrication theory, and axial diffusion of the vapour molecules in the gas. Our formulation includes as limiting cases the diffusion theories of Stefan and Derjaguin et al.

Four independent parameters appear in the theory. One of them, denoted here by χ, is the ratio of the length $L-a$ of the precursor film to the capillary radius a, where L is the length of the gas column. Chapter 3 uses asymptotic analysis to show that the Derjaguin solution correctly determines the total evaporation only for large χ. We use numerical solutions to show that for $\chi \to \infty$, the resistance from taking mass out of the channel must came from the thin film, which explains the success of the Derjaguin solution. A second parameter α is the ratio of the pressure difference $\rho_\ell p_{sat}(1-\phi)/\rho_{sat}$ driving flow in the liquid to the pressure-difference γ/a across the bulk meniscus. Asymptotic analysis of the free boundary problem shows that an apparent contact angle is established for $\alpha/\chi \to \infty$.

Chapter 4 uses numerical solutions to the free boundary problem to test the predictions of asymptotic analysis. Our analysis shows that even though the static contact angle for a completely wetting system is zero, the stationary meniscus of a completely wetting liquid in a channel exhibits an apparent contact angle Θ that is determined chiefly by a capillary number, based on a velocity scale set by evaporation. Though microphysics must be included in the free boundary problem in order to resolve a hydrodynamic singularity at the contact line, Θ is insensitive to the microphysical details.

In appendix B, we describe the numerical scheme used to solve the free boundary problem. Appendix A contains the derivation of major equations.

Chapter 2

Boundary Value Problem

Figure 2.1 shows the geometry of interest. An evaporating meniscus of a completely wetting liquid is formed in the gap between two horizontal flat plates. The plates are held at common temperature T_w equalling that of the surrounding gas. The liquid is chemically pure, but the gas into which the liquid evaporates consists of a mixture of the liquid's vapor and an inert component. Liquid evaporates because the partial pressure of the vapour decreases from its saturation value p_s at the bulk meniscus to ϕp_s at the mouth of the channel. Evaporation draws liquid into the contact region. Near the wetted walls, the resulting pressure differences distort the interface, creating an apparent contact angle, Θ. The length L of the gas column is determined by the initial location of the meniscus; to keep L fixed, liquid is continuously fed into the channel at the same rate $2\dot{m}$ as it is being evaporated.

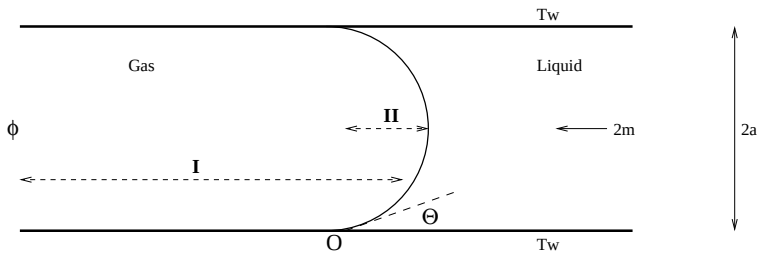

Figure 2.1: The evaporating meniscus in a channel as seen on the scale of the channel gap thickness $2a$. The origin is at O; coordinate axis not shown in the figure.

2.1 Dimensional Equations

We begin with notations: Let μ be the dynamic viscosity, ν the kinematic viscosity, ρ the density, γ the surface tension, ϕ the relative humidity at the channel mouth, A the dispersion constant, p the total pressure within the gas, p_b the bulk liquid pressure, ρ_s the saturation density, R_v the specific gas constant, D_v the binary diffusion coefficient, and $2a$ the channel gap thickness. Subscripts ℓ and v denote the liquid and vapour phases respectively. All properties are evaluated at wall temperature T_w. Lets define;

$$Ca = \frac{\mu_\ell V_\ell}{\gamma}, \qquad V_\ell = \frac{\dot{m}}{\rho_\ell a}, \qquad \Theta_s^2 = \left(\frac{A}{\gamma a^2}\right)^{\frac{1}{3}} \tag{2.1a-c}$$

where Ca is a capillary number based on a velocity scale V_ℓ set by evaporation. Because the liquid is completely wetting, the visible meniscus is preceded by a thin wetting film; we assume that within that film, disjoining pressure Π is related to film thickness h_* by $\Pi = A/h_*^3$. At hydrostatic equilibrium, the wetting film thickness far from the apparent contact line approaches the uniform value $(aA/\gamma)^{1/3}$; Θ_s^2 is the ratio of $(aA/\gamma)^{1/3}$ to the capillary radius a. Since the molecular length scale $(A/\gamma)^{1/2}$ is small compared with the channel gap thickness $2a$, we assume that $\Theta_s^2 << 1$; Renk et al[33] used this disparity in length scales to separate the hydrostatic meniscus into an inner and outer structure, in which an outer semicircular meniscus having radius a matches to an inner solution describing a quasi-parallel wetting film. To ensure that the outer solution is not altered by evaporation, we analyse for the double limit $(\Theta_s^2, Ca) \to 0$; because surface tension is then large, the induced flow can distort the phase interface only within the small scale inner region. We therefore augment the equations posed by Renk et al within the inner region to include both evaporation and diffusion in the gas. Because the induced flow perturbs the interface within the inner region, the vapour partial pressure p_v^* and the liquid pressure p_ℓ^* are obtained, together with the interface shape h^*, by solving the free boundary problem,

$$\dot{m} = \frac{h^{*3}}{3\nu_\ell}\frac{dp_\ell^*}{dx^*} + \frac{aD_v}{R_vT_w}\frac{dp_v^*}{dx^*}, \tag{2.2a}$$

$$p - p_\ell^* = \gamma\frac{d^2h^*}{dx^{*2}} + \frac{A}{h^{*3}}, \tag{2.2b}$$

$$p_v^* = p_s + \frac{\rho_s}{\rho_\ell}(p_\ell^* - p_b); \tag{2.2c}$$

$$p_v^*(a-L) = \phi p_s, \qquad p_v^*(x^* \to a) \to p_s, \tag{2.2d,e}$$

$$h^*(a-L) = \left(\frac{A}{p-p_\ell^*}\right)^{\frac{1}{3}}, \qquad \frac{d^2h^*}{dx^{*2}}(x^* \to a) \to \frac{1}{a} \tag{2.2f,g}$$

Because the mass flow rate $\dot{m}$ is obtained as part of the solution, the capillary number is not known a priori; however, we assume that $Ca \to 0$, and then check for consistency at the end of the analysis. In practice, Θ_s is very small, typically some few 10^{-2}rad for μm-sized channels or less for larger capillaries.

Equation (2.2a) is a statement of mass balance across a cross-section of the channel. It expresses the mass flow rate $\dot{m}$ due to evaporation in the lower half of the channel as the sum of the mass flow rates occurring within the liquid and gas phases. On the right hand side, the first term describes the mass flow due to a Poiseuille flow within the thin quasi-parallel liquid film; the second term describes the mass flow by axial diffusion of vapour through the gas, which is merely the simplified form of Fick's first law,

$$\dot{m}_x = -\frac{aD_v}{R_vT_w}\frac{dp_v^*}{dx^*}, \qquad J^* = \frac{d\dot{m}_x}{dx^*} \tag{2.3a,b}$$

Equation (2.3) neglects the motion induced within the gas mixture; it is a good approximation when the saturation vapour pressure is small compared with the total pressure in the gas. The full form of that equation, including induced motion in the gas, is given as equation (A.10a) in appendix A.3.

Equation (2.2b) is a statement of force balance normal to the interface. It states that the pressure force on an interfacial element balances the resultant force due to capillarity and disjoining pressure. On the right hand side, the first term gives the equation of capillarity for a slowly tapered film, whose slope is significantly small compared with unity; the second term describes the disjoining pressure for a uniform film. Here, the adsorption forces are re-

stricted to the London-van der Waals dispersion forces. Even though Truong and Wayner[30] showed that the inverse cube dependence is appropriate only for film thicknesses less than $20nm$, we use it here as the effects of disjoining pressure become insignificant for film thicknesses greater than that. In the corresponding equation (9) of Deryaguin et al[1], they set $\gamma = 0$. Including surface tension γ allows us to calculate the shape of the whole meniscus.

The kinetic equation (2.2c) is a simplification of the Hertz-Knudsen equation, see the discussion in appendix A.1. It states that liquid and vapour at the interface are in local thermodynamic equilibrium; as a result, the rate-limiting step controlling evaporation is the stationary diffusion of the vapour molecules in the surrounding gas. Liquid temperature differences induced by evaporation have been assumed kinetically negligible; the system is effectively isothermal for the slow evaporation processes considered in this analysis.

Boundary condition (2.2d) fixes the vapour pressure at the channel mouth. Boundary condition (2.2f) on the film thickness at the channel mouth is obtained by neglecting capillarity in equation (2.2b). The other two boundary conditions, equations (2.2e,g), are obtained by matching the outer limit of the lubrication solutions to the inner limit of the outer solutions. Specifically, boundary condition (2.2g) ensures that the interface curvature at the outer edge of the lubrication region matches smoothly to the uniform curvature of the outer circular arc meniscus; the other boundary condition (2.2e) is a matching condition on the vapour partial pressure. The vapour pressure at the outer edge of the lubrication region is equal to the saturation pressure because for vanishing capillary numbers, changes in liquid pressure along the outer meniscus are negligibly small. Therefore $p_\ell^* = p_b$ to a first approximation, and it follows from equation (2.2c) that $p_v^* = p_s$ along the outer meniscus. Because the film thickness grows parabolically with distance, according to (2.2g), the effects of disjoining pressure are insignificant at the outer edge of the lubrication region. Therefore, the outer limit of the normal stress equation (2.2b) requires that we chose the bulk liquid pressure to be

$$p_b = p - \gamma/a, \tag{2.4}$$

This same boundary condition is used by Deryaguin et al[1], see their equation (11), even though their boundary value problem does not include capillarity, and therefore does not match smoothly to the outer circular arc meniscus.

Equation (2.2a,b) is related to that of Hervet et al (1984, Eq 5)[39] in that

they are both limiting cases of a spreading volatile meniscus. Whereas we neglect boundary motion and study the evaporating stationary meniscus; they neglect evaporation and study the spreading isothermal meniscus.

2.2 Dimensionless Equations

We non-dimensionalize (2.2) by letting,

$$h_s = a\Theta_s^2, \qquad x_s = a\Theta_s \tag{2.5a,b}$$

where the slope unit Θ_s is defined in (2.1c); it is proportional to Θ, and measures the ratio of the molecular length scale $\sqrt{A/\gamma}$ to the channel gap thickness $2a$. For $\phi = 1$, there is no evaporation; for this case, the wetting film approaches a uniform value h_s far from the apparent contact line. x_s is the horizontal length scale at which capillarity balances disjoining pressure, when the film thickness is of order h_s. Using the above choice for scales, we introduce dimensionless variables (without asterisks) by

$$p_\ell = \frac{a}{\gamma}(p_\ell^* - p_b), \qquad x = \frac{x^*}{x_s}, \qquad h = \frac{h^*}{h_s}. \tag{2.6a-c}$$

To non-dimensionalize (2.2), we first eliminate the vapour pressure in favour of the liquid pressure using equation (2.2c); then substituting (2.6) into the resulting problem (2.2), we find that the unknowns h and p_ℓ satisfy the following dimensionless boundary value problem: for $-\chi \le x\Theta_s < 1$,

$$\frac{d}{dx}\left[\left(\frac{h^3}{3} + \beta\right)\frac{dp_\ell}{dx}\right] = 0, \tag{2.7a}$$

$$1 - p_\ell = \frac{d^2h}{dx^2} + \frac{1}{h^3}; \tag{2.7b}$$

$$p_\ell(-\chi/\Theta_s) = -\alpha, \qquad p_\ell(x \to 1/\Theta_s) \to 0, \tag{2.7c,d}$$

$$h(-\chi/\Theta_s) = \left(\frac{1}{1+\alpha}\right)^{\frac{1}{3}}, \quad h(x \to 1/\Theta_s) \to \frac{x^2}{2} \tag{2.7e,f}$$

Equation (2.7a) has been differentiated once so as to eliminate the integration constant $\dot{m}$. The interface curvature cannot be prescribed as a boundary condition because the differential equations are second order in h^*; as a result, matching condition (2.2f) on the interface curvature far from the apparent contact line is integrated and replaced with (2.7f). Because the independent variable now appears explicitly in the boundary condition, the problem is no longer autonomous; as a result, the origin is fixed at the apparent contact line and can no longer be arbitrarily chosen. Because $\Theta_s << 1$, the matching conditions (2.7d,f) are imposed at $x \to \infty$. Four independent parameters appear in the dimensionless boundary value problem; α, β, χ, and Θ_s.

$$\alpha = \frac{a\rho_\ell}{\gamma\rho_s} p_s(1-\phi), \qquad \beta = \frac{\nu_\ell \rho_s \gamma D_v}{\rho_\ell R_v T_w A}, \qquad \chi = \frac{L-a}{a} \tag{2.8a-c}$$

According to equations $(2.2c, d, e)$, the liquid pressure decreases from p_b at the bulk meniscus to $p_b - \rho_\ell p_s(1-\phi)/\rho_s$ at the channel mouth; the parameter α is the ratio of the pressure-difference $\rho_\ell p_s(1-\phi)/\rho_s$ driving the resulting liquid flow to the pressure-difference γ/a across the bulk meniscus. For fixed α and position x, the parameter β controls the fraction of the total mass flow transported by axial diffusion in the gas. The other parameter χ measures the aspect ratio of the channel. For use in subsequent analysis, we define

$$f = \frac{\dot{m}}{\dot{m}_s}, \qquad \dot{m}_s = \frac{aD_v p_s}{R_v T_w L}(1-\phi), \qquad \omega = \frac{\alpha}{\chi}\Theta_s \tag{2.9a-c}$$

According to the simplified form of Fick's law, $\dot{m}_s$ is the diffusive transport caused by a gradient $(1-\phi)p_s/L$ of vapour concentration. The integration constant f is the ratio of the total evaporation from the capillary to $\dot{m}_s$. The parameter ω is the ratio of pressure gradients driving flow within the contact region to pressure gradients driving flow within the bulk meniscus.

Table 2.1 shows representative values for the parameters in the theory. The table uses $A = 10^{-21} J$ for the dispersion constant, $\phi = 0.3$ for the relative humidity in the distant gas, $L = 50\mu m$ for the length of the gas column, and $a = 10\mu m$ for the capillary radius. The size of β is very sensitive to the value of the dispersion constant; $0.01 < \beta < 1$ whereas α is generally large.

Liquid	$10^{-4}\alpha$	β	Θ_s	ω
$Heptane$	0.5529	0.2072	0.0282	38.9394
$Octane$	0.4550	0.3107	0.0277	31.5431
$Water$	1.3280	0.2113	0.0228	75.5533

Table 2.1: Estimates of parameters

Chapter 3

Asymptotic Analysis

This chapter studies the parameter rich problem (2.7) for special limiting values of the parameters. The results of that asymptotic analysis are tested against numerical solutions to the complete problem in chapter 4

3.1 Analysis for $\chi \to \infty$ with Θ_s fixed

For $\chi \to \infty$ with Θ_s fixed, the length of the gas column becomes significantly larger than the channel gap thickness. This disparity in length scales gives the theory an inner and outer structure. Within the long inner thin film region, the governing equations simplify because capillarity is negligible. The simplified equations are identical to those posed by Derjaguin et al[1]. We simplify the outer analysis by assuming that the pressure within the outer region is uniform, equalling the bulk liquid pressure, even though the inner problem does not describe the bulk meniscus. We revisit this approximation in the next chapter, where we point out when it breaks down. For now, we establish the above structure for the meniscus on the lower wall using asymptotic analysis for large χ. To begin, the governing equations are rescaled using the inner variable $\xi = x\Theta_s/\chi$ to show that for $\chi \to \infty$ with Θ_s fixed, we get

$$\left(\frac{h^3}{3\beta} + 1\right)\frac{dp_\ell}{d\xi} = \alpha f, \quad 1 - p_\ell = \frac{1}{h^3}; \quad with \quad p_\ell(-1) = -\alpha \qquad (3.1\text{a-c})$$

and a matching condition at $\xi \to 0$, to be determined. The mass balance equation (2.7a) has been integrated once, with $\alpha\beta f\Theta_s/(\chi+1)$ the integration

constant. The total mass flow f, a constant, is determined by matching the inner solution to the outer solution. Because capillarity is negligible, liquid flow within the inner region is driven by gradients in disjoining pressure only. Because the inner problem (3.1) is identical to the boundary value problem posed by Derjaguin et al[1], we shall occasionally refer to its solution as the Derjaguin solution. Integration shows that the liquid pressure p_ℓ satisfies,

$$\log\left(\frac{1+\alpha}{1-p_\ell}\right) + 3\beta\,(\alpha + p_\ell) = 3\alpha\beta f\,(\xi + 1) \tag{3.2}$$

Since the inner solution (3.2) does not describe the bulk meniscus, one will need a boundary condition on the liquid pressure at the outer edge of the inner region in order to determine f. That boundary condition is obtained by solving an outer problem, and then matching to the inner solution. To simplify that outer analysis, we assume that the pressure within the outer region is uniform, equalling the liquid pressure at the bulk meniscus. Matching then requires that boundary condition (2.7d) on the liquid pressure at the bulk meniscus be imposed at the outer edge of the inner region; i.e,

$$p_\ell \to 0 \qquad as \qquad \xi \to 0 \tag{3.3}$$

The identical boundary condition is used by Derjaguin et al[1], consult their equation (11). The results of this section are therefore going to be identical to those already reached at by Derjaguin et al, the difference being that our analysis is systematic. Equations (3.1b) and (3.3) predict a maximum film thickness that is equal to the precursor film thickness for hydrostatic equilibrium. The film thickness in the inner region therefore decreases from a maximum of $h = 1$ at the outer edge to a minimum of $h = (1+\alpha)^{-1/3}$ at the channel mouth. We now imposed the matching condition (3.3) onto the inner solution (3.2) to show that the total evaporation from the capillary,

$$\frac{\dot{m}}{\dot{m}_s} = 1 + \frac{\log(1+\alpha)}{3\alpha\beta} \qquad as \qquad \chi \to \infty \tag{3.4}$$

According to equation (3.4), with increasing α, the ratio $\dot{m}/\dot{m}_s$ decreases monotonically from its maximum value of $1+1/3\beta$ at $\alpha = 0$; by its definition

(2.8a), $\alpha \to 0$ corresponds to $a(1-\phi) \to 0$; as concluded by Derjaguin et al, the effect of the precursor film is most significant for capillaries of small radius a when the system is near hydrostatic equilibrium ($\phi \to 1$). As α is reduced, the film thickness at the exit is increased. According to (2.7a), transport along the liquid film varies as h^3; doubling h increases the film transport by almost an order of magnitude. This explains the increased contribution from the precursor film as $\phi \to 1$ or as the bulk meniscus is reduced in size.

3.2 Analysis for $\omega \to \infty$ with β fixed

Liquid flows from the bulk meniscus into the contact region in order to replenish mass lost from evaporation. For $\alpha \to \infty$, with the channel length fixed, the flow becomes strong enough to distort the interface, and as a result, creates an apparent contact angle, Θ. Increasing the channel length reduces the value of Θ because pressure gradient driving diffusion in the gas, and hence the liquid flow, reduces as we increase the length of the gas column. We therefore expect Θ to be an increasing function of ω. To prove that, we carry out an asymptotic analysis for large ω, with the parameter β fixed.

Figure 3.1 outlines the structure of the meniscus that we are about to establish for the contact region on the lower wall. For $\omega \to \infty$ with β fixed,

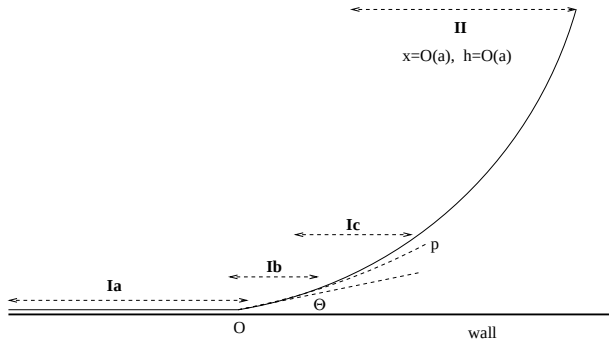

Figure 3.1: Structure of the meniscus on the lower wall for $\omega \to \infty$.

the inner lubrication region can be systematically divided into three sub-regions. Sub-region Ia describes the Stefan diffusion model. Sub-region Ic is described by a parabolic arc meniscus, above which the gas is saturated with the liquid's vapour. For $\omega \to \infty$, evaporation occurs within the intermediate

region Ib, where the apparent contact angle Θ is also established. The above structure is now established using asymptotic analysis for large ω.

To begin, we rescale (2.2) by letting

$$\eta_s = a\beta^{\frac{1}{3}}\Theta_s^2, \qquad \xi_s = a\Theta_s\left(\frac{\beta^{\frac{1}{3}}}{\omega}\right)^{\frac{1}{3}}, \qquad \Delta p = \frac{\gamma}{a}\left(\omega^2\beta^{\frac{1}{3}}\right)^{\frac{1}{3}} \tag{3.5a-c}$$

The scales suggested in equation (3.5) ensures that all three terms in the mass balance equation (2.2a) are comparable when the film thickness, horizontal length scale, and pressure differences across the interface are respectively of order η_s, ξ_s and Δp. Physically, η_s is the film thickness at which a Poiseuille flow within the liquid film balances diffusion in the gas; ξ_s the tangential length scale at which evaporation balances the divergence in mass flow rate, when pressure differences across the interface are of order Δp. For a mm-sized channel, we find that $\xi_s \simeq 0.5\mu m$ and $\eta_s \simeq 15nm$; whereas for a μm-sized channel, both length scales are typically some few nanometres.

Next, we define intermediate variables by

$$\eta = \frac{h^*}{\eta_s}, \qquad \xi = \frac{x^*}{\xi_s}, \qquad p = \frac{p_\ell^*}{\Delta p} \tag{3.6a-c}$$

Substituting the intermediate variables into problem (2.2), and then take the limit as $\omega \to \infty$ with β fixed, we find that the unknowns η and p satisfy the following dimensionless boundary value problem: for $-\infty < \xi < \infty$,

$$\left(\frac{\eta^3}{3} + 1\right)\frac{dp}{d\xi} = f, \quad -p = \frac{d^2\eta}{d\xi^2}; \quad with \quad \eta''(\infty) = 0 \tag{3.7a-c}$$

Equations (3.7) are supplemented with matching conditions at $-\infty$, to be determined. The constant f is defined in (2.9). The domain is the real line because $\xi \to \infty$ as $\omega \to \infty$ with x fixed. The limit $\omega \to \infty$ is singular for two reasons: first, disjoining pressure is negligible; an inner region Ia is therefore necessary to satisfy the thin film boundary conditions. Secondly, because the interface curvature vanishes at ∞, problem (3.7) does not describe the parabolic arc meniscus. An outer region Ib is therefore necessary; otherwise, matching to the circular arc meniscus will be impossible. The intermediate

problem is thus defined by (3.7), and integration shows that for $\xi \to \infty$,

$$\frac{d\eta}{d\xi} = k - \frac{3f}{2k^3}\xi^{-1} + o\,(1)\ , \qquad p = -\frac{3f}{2k^3}\xi^{-2} + o\,(1) \tag{3.8a,b}$$

We give equation (3.8b) to stress that the vapour pressure approaches its saturation pressure at the outer edge of the intermediate region. Pressure gradients driving diffusion above the parabolic arc meniscus are therefore asymptotically negligible; as a result, the total evaporation from the parabolic arc meniscus is negligibly small. Evaporation thus occurs within the intermediate region. On a similar note, we give the second term on the right hand side of equation (3.8a) to stress that the slope approaches a limit at infinity. Because the slope approaches a limit at the outer edge of the intermediate region, a contact angle is established there. Specifically, $\Theta = b\Theta_s$, where

$$b \to k\omega^{1/3}\beta^{2/9} \qquad as \qquad \omega \to \infty \tag{3.9}$$

We have used the definition $\Theta = h^*_{x^*}$ and equation (3.8a). The integration constant k can be found by solving the intermediate problem, subject to matching conditions at minus infinity. However, we take a different approach; we instead obtain k using numerical solutions to (2.7), see §4.2. Because the parameter β is independent neither on ϕ nor on L, the solutions to the intermediate problem can only be a function of β as $\omega \to \infty$. Consequently, the constant $k = k(\beta)$ only, independent on ω. This point is very important because as we shall see in chapter 4, it guides us in choosing the scaling necessary for collapsing the numerical solutions onto a single curve. We define a capillary number Ca, based on a velocity scale V_s set by evaporation, as

$$V_s = \frac{p_s(1-\phi)}{L-a}\left(\frac{aD}{\rho_\ell R_v T_w}\sqrt{\frac{\rho_\ell}{\mu_\ell \rho_s}}\right)^{\frac{2}{3}}, \qquad Ca = \frac{\mu_\ell V_s}{\gamma} \tag{3.10a,b}$$

Observe that the dispersion constant A doesn't appear in the definitions of the velocity scale and capillary number. This observation is used below to show that micro-physics affects Θ only through the constant k. To begin, we obtain a relation between contact angle and capillary number by substituting the definition (3.10) of Ca into the scaling relation (3.9) to show that,

$$\Theta = kCa^{1/3} \qquad where \qquad k = k(\beta) \tag{3.11}$$

Because the capillary number is not a function of the dispersion constant, micro-physics affects Θ only through the constant $k = k(\beta)$; we recall that the definition (2.8b) of β contains the dispersion constant A. This result is tested in the next chapter using numerical solutions to (2.7) without approximation.

Similarly, the channel size affects Θ only through the capillary number. The functional relationship between Θ and capillary size must however be explained with caution: For a channel, the length of the wetting film is of order of the channel length, and as a result, $\Theta \propto (a^{2/3}/L)^{1/3}$; for a droplet, the length of that film is of order of drop size, and as a result, $\Theta \propto a^{-1/9}$.

Chapter 4

Numerical Results and Discussion

The governing equations (2.7) are numerically solved using the NAG routine D02TKF, which uses the collocation method to approximate the solution at certain specified locations within the problem domain; solution values at anywhere else within the domain are obtained using polynomial interpolation. The routine uses variable steps in x with deferred correction. Because the slope unit $\Theta_s << 1$, we solve for $\Theta_s \to 0$; and for $\alpha \to \infty$ because then a contact angle is established. These limiting solutions complicate the analysis for the following two reasons: first, the resulting system of non-linear algebraic equations, for the coefficients of the basis functions, becomes very ill-conditioned as $\alpha \to \infty$; secondly, the problem domain becomes infinite in the limit as $\Theta_s \to 0$. This work alleviates both difficulties by using continuation in the parameters α and Θ_s. The equations are first mapped onto the open interval $[-\chi, 1)$ using the transformation $\hat{x} = x\Theta_s$, which is equivalent to using $\hat{x} = x^*/a$. We use the closed interval $[-\chi, x_1]$ in the computations, where the distance x_1 is chosen such that $0 << x_1 < 1$. The solutions are independent on the value of x_1, so long as it is not too far from unity.

Next, we describe the numerical scheme: Numerical solutions are first obtained for the hydrostatic case $\alpha = 0$ and $\Theta_s > 0$ using the initial approximations; $p = 0$ and $h = 1$. The obtained solutions are then used as initial guesses in the solution for $\alpha = \alpha + \Delta\alpha$ and $\Theta_s = \Theta_s - \Delta\Theta_s$. The process is repeated until we obtain solutions for the values α and Θ_s that we desire. If that value of Θ_s is not too small, then continuation in Θ_s is unnecessary. For a desired value of $\Theta_s \to 0$, continuation must be used in order to avoid a

possible numerical singularity in the Jacobian used in the Newton iteration. The numerical scheme is discussed and presented at length in chapter B.

Figure 4.1 compares the numerical solution of problem (2.7) without approximation with the asymptotic solution (3.2) of Derjaguin et al. Within the long slowly tapered section of the meniscus, capillarity is negligible. This explains the good agreement between the two solutions in that part of the meniscus. The agreement also confirms the robustness and accuracy of our

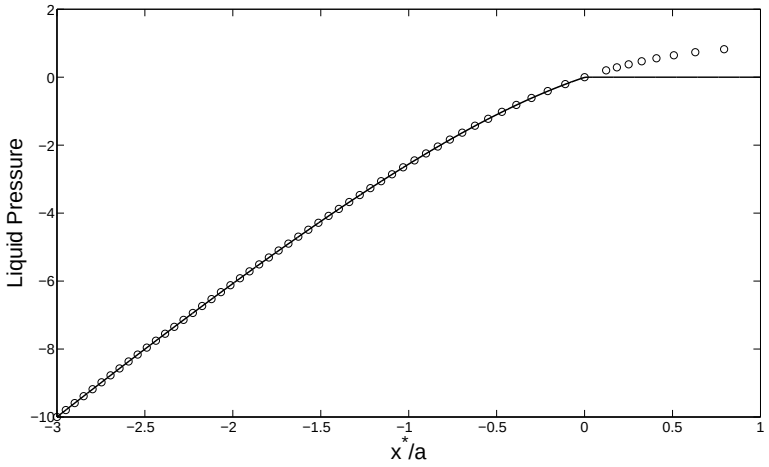

Figure 4.1: Liquid pressure $(p_\ell^* - p_b)a/\gamma$ as a function of position x^*/a: open circles, equation (3.2); solid curve, computed without approximation from (2.7). With $\chi = 3$, $\alpha = 10$, $\beta = 0.2$, and $\Theta_s = 0.01$: for χ, α, β, and Θ_s, see (2.8) and (2.1) respectively.

numerical scheme. It is also clear from the figure that the Derjaguin solution correctly describes the meniscus up to the apparent contact line.

In the thermal model, DasGupta et el[26] integrate the governing equations using the shooting method. This problem differs from the thermal problem because the solution continues to depend on both constants in the starting series. It is for this reason that we decided to solve the problem as a boundary value problem. One consequence of solving the problem as a boundary value problem is that the contact angle cannot be directly obtained from the model problem using a local analysis around the contact region; unless the slope parameter is obtained using some iterative process. It is for this reason that we scale the problem, making sure that the interface curvature does not vanish at the outer edge of the problem domain. Once the numerical

solutions are obtained on these set of scales, the apparent contact angle can then be extracted from the computed values of h as explained in section 4.2.

4.1 The total evaporation $\dot{m}$

Figure 4.2 compares the total evaporation from the capillary computed without approximation from problem (2.7) with the approximate solution of Derjaguin et al, equation (3.4). We observe that the numerical solution asymptotically approaches the Derjaguin solution as $\chi \to \infty$, irrespective of the size of the parameter β. This result is consistent with the asymptotic analysis of

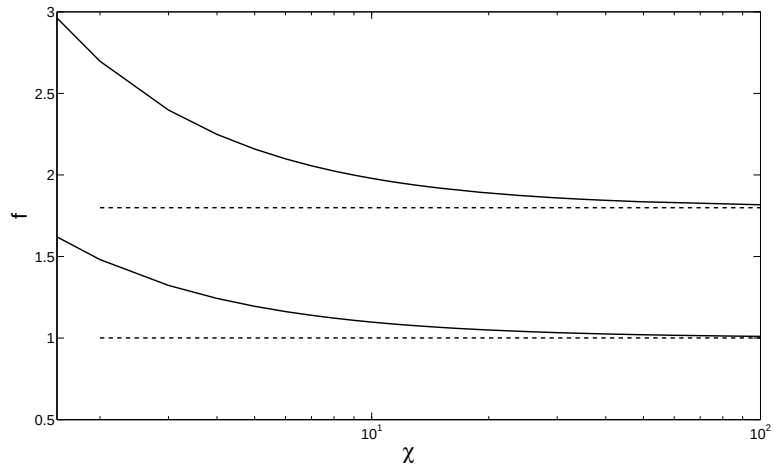

Figure 4.2: Mass flow $f = \dot{m}/\dot{m}_s$ computed from (2.7) without approximation as a function of channel length χ: $\alpha = 10$; $\Theta_s = 0.008$; bottom curves, $\beta = 100$; top curves, $\beta = 0.1$. The limiting solutions, dotted lines, are computed using the Derjaguin solution, equation 3.4, for the same α and β. For α, β, and $\dot{m}_s$, see (2.8) and (2.9) respectively.

section 3.1 which claims that for χ large and arbitrary β, the Derjagun solution is sufficient for computing the total evaporation from capillaries. The graph shows the numerical solution departing from the Derjaguin solution as the parameter $\chi \to 1$. The large departure means that the Derjaguin solution significantly under-estimates the total evaporation from the capillary, when the length of the gas column is comparable to the capillary radius.

Figure 4.3 shows the vapour pressure computed from (2.7) without approximation as a function of position along the channel. The figure shows

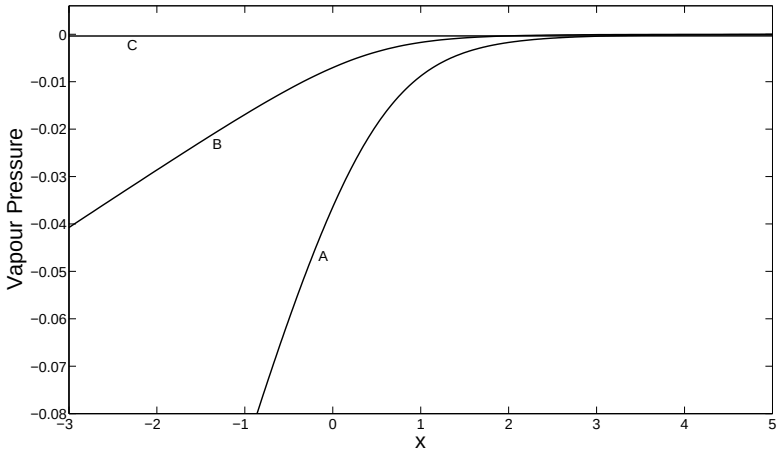

Figure 4.3: Vapour pressure $(p_v^* - p_s)a\rho_\ell/\gamma\rho_s$ as a function of position x^*/x_s. The curves are computed without approximation from problem (2.7) using $\chi = 1$, curve A; $\chi = 5$, curve B; and $\chi = 100$, curve C. With $\alpha = 10$, $\Theta_s = 0.01$, and $\beta = 0.3$ all fixed. For the definitions of χ, α, β, and Θ_s, see equations (2.8) and (2.1) respectively

that as χ is increased, the pressure becomes uniform over an increasing portion of the channel length. For fixed α, increasing the channel length reduces pressure gradients driving diffusion in the gas. As a result, both diffusion along the gas column and film flow becomes slow. Because it is then difficult to remove vapour from the meniscus, the pressure becomes uniform over a distance that is an increasing function of L. Consequently, more and more of the resistance to taking mass out of the channel must came from the thin wetting film as L increases. This explains why the Derjaguin solution correctly determines the total evaporation for large χ, see figure 4.2.

Figure 4.4 shows the evaporative mass flux J normal to the interface as a function of position along the wall, with β as a parameter. As can be seen from the graphs, evaporation is shifted into the thicker portions of the meniscus as β increases. This means that evaporation from the precursor film decreases as β increases, which is consistent with the approximate solution of Derjaguin et al. Physically, liquid flows from the bulk meniscus into the thin film region to compensate for evaporation. Because β is proportional to liquid viscosity, increasing β increases the viscous resistance to the compensatory flow; as a result, liquid is prohibited from flowing into the

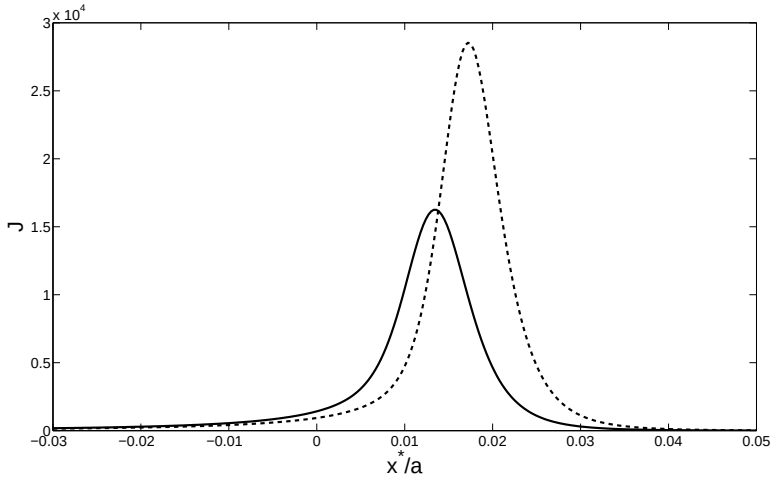

Figure 4.4: Evaporative mass flux $J^*\nu_\ell/(\gamma\Theta_s^4)$ computed from (2.7) without approximation as a function of position x^*/a using $\alpha = 2000$, $\chi = 2$, and $\Theta_s = 0.01$: solid curve, $\beta = 0.2$; dotted line, $\beta = 0.3$. See equations (2.1), (2.5) and (2.8) for the parameters.

precursor film. Reducing β lowers the viscous resistance, thereby increasing evaporation from the precursor film. Consequently, for fixed α, β controls the distribution of evaporation along the meniscus; by equation (2.7a), evaporation occurs at a film thickness that is of order $\beta^{1/3}$. For $h^3 << \beta$, evaporation ceases because transport in the liquid film becomes negligibly small, making transport along the gas column independent on x. Towards the bulk meniscus, evaporation ceases because the pressure above the outer visible meniscus is uniform, equalling the saturation pressure p_s. Here, we are assuming that the capillary number, based on the velocity of the induced flow, is negligible.

Given the above argument about β, one would have expected the inner problem (2.7) to break down as $\beta \to \infty$; because then, evaporation will be occurring at a film thickness large compared with the inner dimensions. However, this is not the case, because as we explained above, pressure gradients above the outer meniscus are negligibly small. This explains why all the evaporation occurs within the inner region, irrespective of the size of β. The large value of β used in computing figure 4.2 is to demonstrate this fact.

4.2 The apparent contact angle, Θ

According to boundary condition (2.2f), the interface curvature approaches a constant at the outer edge of region I; the film thickness thus grows parabolically with distance as $x \to \infty$. If the parabola so defined has a zero, then a contact angle is defined by the slope at $h = 0$. Since the entire interface does not have a constant curvature, an apparent contact angle is defined by first computing the constant curvature profile for large h, and then extrapolate down to $h = 0$. To give a precise definition of Θ using this method, we follow Morris[36] and multiply the asymptotic relation $d^2h/dx^2 \sim 1$ by $2dh/dx$, and then integrate once in x to show that $(dh/dx)^2 \sim 2h + b^2$, where b^2 is the integration constant. We therefore define the contact angle $\Theta = b\Theta_s$, where

$$b^2 = \lim_{\omega\to\infty} \lim_{h\to\infty} \left(h_x^2 - 2h\right) \tag{4.1}$$

The integration constant b is equivalent to the constant b defined in the asymptotic relation (3.9); we refer to b as the slope parameter. In (4.1), the outer limit $\omega \to \infty$ ensures that the liquid flow is strong enough to create an apparent contact angle. The other limit $h \to \infty$ picks out the constant curvature part of the interface, and also ensures that the apparent contact angle defined by equation (4.1) is independent of film thickness. Numerical solutions are now used to establish the existence of a contact angle.

Figure 4.5 shows d^2h/dx^2 computed from (2.7) without approximation as a function of h; as defined by (2.9), $\omega = \alpha\Theta_s/\chi$ is proportional to the potential difference $p_s(1-\phi)$ driving evaporation. On the right hand side of the figure, $d^2h/dx^2 \to 1$, as required by boundary condition (2.7f). Near the origin, however, $d^2h/dx^2 \to 1$ has a local maximum for 3 of the 4 curves. The maximum value is an increasing function of the driving potential difference. Physically, for $\omega > 0$, liquid flows from the bulk meniscus into the contact region to compensate for evaporation. For $\omega \to 0$, the flow is too weak to alter the interface shape, bottom curve. For $\omega \to \infty$, however, the flow becomes strong enough to perturb the interface, and creates an apparent contact angle. Figure 4.5 thus supports the outer limit defined in (4.1).

In figure 4.6, we show $(dh/dx)^2$ computed from (2.7) without approximation as a function of h; as expected, $(dh/dx)^2$ is an increasing function of the driving potential difference. On the right hand side of the figure, we observe that $(dh/dx)^2$ grows linearly with h; consistent with a constant curvature

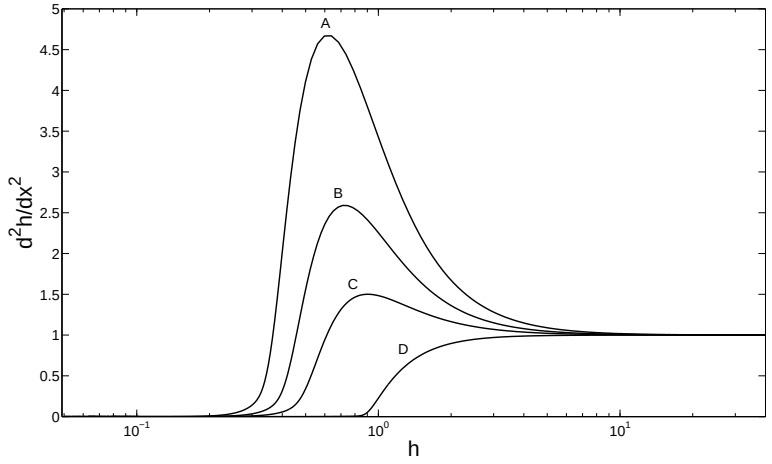

Figure 4.5: Interface curvature $a(d^2h^*/dx^{*2})$ computed without approximation from the inner problem (2.7) as a function of film thickness $h = h^*/h_s$. The curves represent values computed for: A, $\omega = 40$; B, $\omega = 20$; C, $\omega = 10$; D, $\omega = 0.5$; using $\beta = 0.2$. The length scale h_s is defined in (2.5) while parameters ω and β are defined in equations (2.8,2.9).

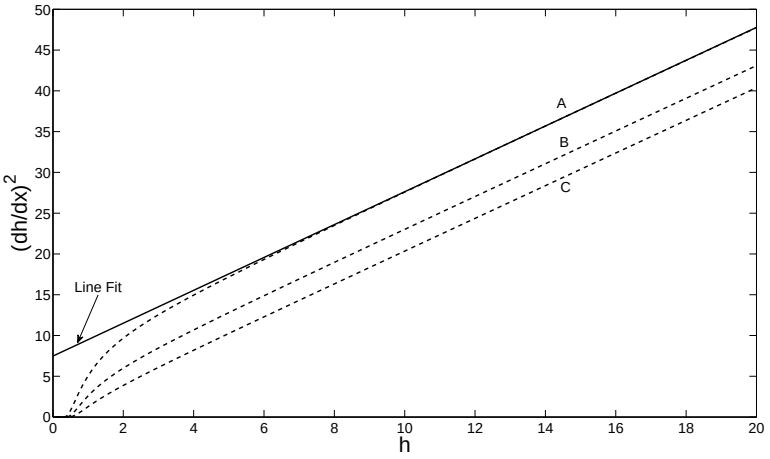

Figure 4.6: Squared interface slope $(\gamma a^2/A)^{1/3}(dh^*/dx^*)^2$ computed without approximation from the inner problem (2.7) as a function of film thickness $(\gamma/aA)^{1/3}h^*$. Broken curves represent values computed for: A, $\omega = 40$; B, $\omega = 20$; C, $\omega = 10$. These are the same values used in figure 4.5, with $\beta = 0.2$. The solid line represents a line fit for large h, using the least square method. See definitions (2.8,2.9) for the parameters ω and β.

region. The figure shows that the interface curvature becomes uniform only for film thicknesses $h > 10$. Therefore to extract b from the computed values of h, we first discard all data for $h < 10$, and then fits a straight line to the rest using the least square method. The intercept of that line determines b^2.

Figure 4.7 shows b as a function of $\omega^{1/3}\beta^{2/9}$. The choice for the independent variable $\omega^{1/3}\beta^{2/9}$ is suggested by the scaling relation (3.9). According to that scaling relation, a plot of b against $\omega^{1/3}\beta^{2/9}$ should give a straight line, whose slope k is a function of β. The small scatter in the numerical solutions is a clear indication that k is a very weak function of β. We therefore take advantage of that information and plot b as a function of $\beta^{\delta}\omega^{1/3}\beta^{2/9}$, where the exponent δ is chosen, by trial and error, so as to collapse all the numerical solutions onto a single straight line. Based on figure 4.7, we expect $\delta \to 0$.

Figure 4.8 shows that the choice $\delta = 4/225$ collapses the numerical solutions onto a single straight line as $\omega^{1/3}\beta^{6/25} \to \infty$; this implies that the slope parameter $b \to s\omega^{1/3}\beta^{6/25}$ as $\omega^{1/3}\beta^{6/25} \to \infty$, where s is the slope of the line. The figure shows that the numerical solutions collapse onto the straight line only for values of $\omega^{1/3}\beta^{6/25} > 3$. Therefore, to obtain s from the numerical solutions, we first discard all data for $\omega^{1/3}\beta^{6/25} < 3$, and then fits a line to the rest using the least square method. The slope of that line determines s. Using this method, we find that $s \simeq 1.76$. The related expression for b is

$$b \to 1.76\omega^{1/3}\beta^{6/25} \qquad as \qquad \omega^{1/3}\beta^{6/25} \to \infty \tag{4.2}$$

Comparing this result to the scaling relation (3.9), we find that the integration constant $k = 1.76\beta^{4/225}$, which is a very weak function of β as suggested in figure 4.7. Equation (4.2) provides a useful correlation between b, ω, and β. The corresponding expression for Θ, following equation (3.11), is

$$\Theta = kCa^{1/3} \qquad where \qquad k = 1.76\beta^{4/225} \tag{4.3a,b}$$

Figure 4.9 shows k as a function of β. The graph shows that the contact angle depends very weakly on micro-physics, except for $\beta \to 0$. Physically, the film thickness at which the contact angle is established is proportional to the parameter $\beta^{1/3}$. Therefore for $\beta \to 0$, the contact angle is established at the scale where disjoining pressure is significant. This also explains why the contact angle varies weakly with β for large β; here, Θ is established at

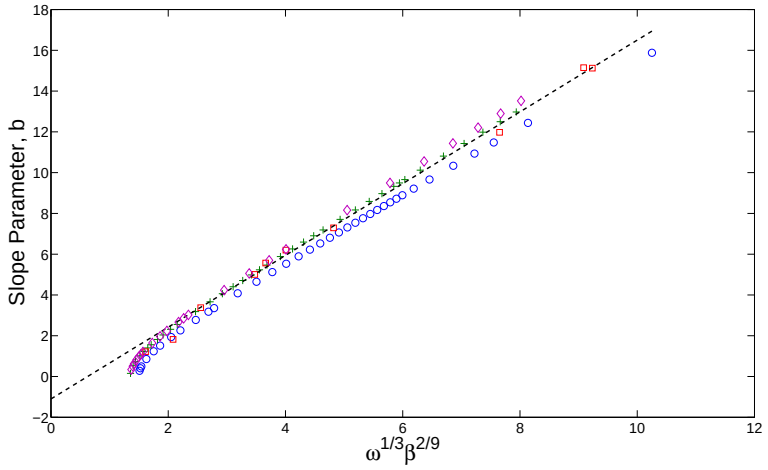

Figure 4.7: Slope parameter b as a function of the parameter $\omega^{1/3}\beta^{2/9}$: Symbols denote values computed without approximation from problem (2.7) using the definition (4.1) of b: Triangles, $\beta = 10$; open circles, $\beta = 0.1$; plus sign, $\beta = 1$; and squares for selected values of β between 0.01 and 30. These values include the range typical in applications.

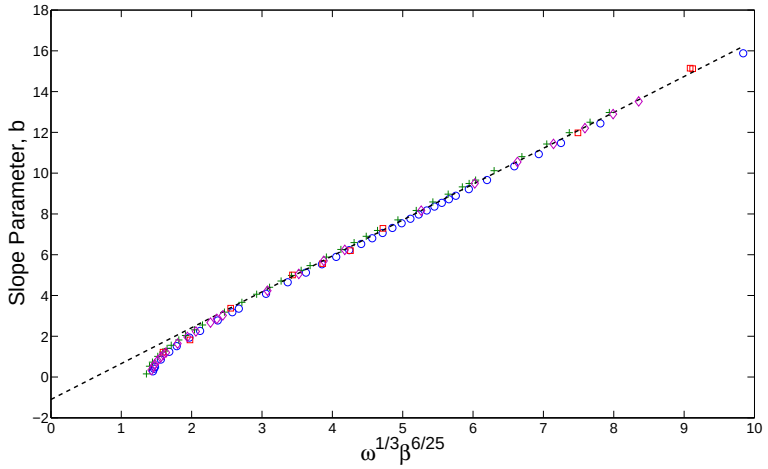

Figure 4.8: Slope parameter b as a function of the parameter $\omega^{1/3}\beta^{6/25}$: Symbols denote values computed without approximation from problem (2.7) using the definition (4.1) of b: Triangles, $\beta = 10$; open circles, $\beta = 0.1$; plus sign, $\beta = 1$; and squares for selected values of β between 0.01 and 30. These values include the range typical in applications.

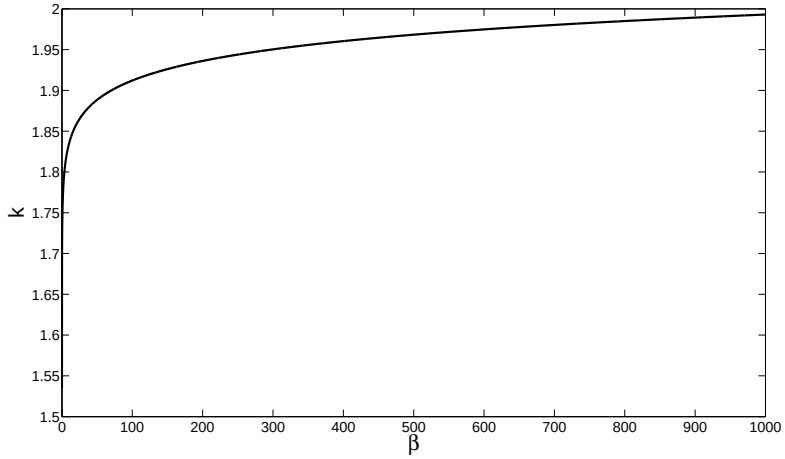

Figure 4.9: Effects of micro-physics on Θ.

a scale where disjoining pressure is insignificant. These effects can also be explained by first noting that β measures the viscous resistance to liquid flow; which implies that for large β, liquid motion, and hence the distortion of the interface, occurs at a much larger scale than that at which disjoining pressure is significant. Figure 4.9 covers a sufficiently wide range of β, including the range typical in applications. Specifically, it covers $10^{-3} \leq \beta \leq 10^{3}$, and the figure shows that over this range of β, the integration constant

$$1.5 < k < 2.0 \qquad so\ that \qquad \Theta = 1.75 Ca^{1/3} \tag{4.4a,b}$$

with very little error. Equation (4.4b) expresses the apparent contact angle as a function of a single parameter Ca depending only on well-known macro-physical properties. The finding that Θ is insensitive to microphysics has been obtained for the thermal problem by Stephan et al[34] and by Morris[36].

Chapter 5

Conclusion

In the title problem, a completely wetting pure liquid with uniform surface tension γ evaporates into a binary mixture consisting of its own vapour and an inert component. Because the system is completely wetting, the visible meniscus is preceded by a wetting film; we assume that within this film, disjoining pressure Π is related to film thickness h by $\Pi = A/h^3$, where A is the dispersion constant. Together A and γ define a length scale $(A/\gamma)^{1/2}$; this length scale is of molecular dimensions. The extended meniscus consisting of the visible meniscus and its precursor film occupy a channel of gap thickness $2a$; we assume that the gap is large compared with the molecular scale; $1 \gg [A/(a^2\gamma)]^{1/2}$. At the channel exit, the partial pressure of the vapour is ϕp_s, where p_s is the saturation pressure at the uniform temperature T_w of the channel walls. For $\phi = 1$, the system is in hydrostatic equilibrium; for this case, Renk et al[33] show that for $1 \gg [A/(a^2\gamma)]^{1/2}$ the extended meniscus has an inner–and–outer structure: the outer visible meniscus is a semicircle of radius a; the inner solution consists of a non–uniform wetting film in which the capillary and disjoining pressures are comparable in magnitude. Far from the apparent contact line, the thickness of the wetting film approaches the uniform value $(aA/\gamma)^{1/3}$; this thickness is, of course, small compared with a. In this thesis, we have analysed the effect of evaporation on that picture.

For $\phi < 1$, the partial pressure at the exit is less than the value required for the liquid to coexist in equilibrium with its vapour. As a result, liquid evaporates from the extended meniscus. Though heat must be conducted from the walls to the liquid–vapour interface to drive evaporation, we have assumed that in the presence of the inert component, mass transfer along the gas column is rate–limiting. Consequently, we have assumed the system

to be isothermal; this approximation is justified in Appendix A.2.

To analyse the evaporating meniscus, we have used the separation of scales described above. The inner region now consisting of the quasi–parallel liquid film, and the corresponding portion of the gas column. Within this region, the lubrication approximation holds within the film and, across the gas column, the partial pressure is uniform. Owing to these two conditions, the unknowns depend only on distance along the wall, and the mass transport within the inner region is determined by the boundary value problem (2.2) containing only ordinary differential equations. For the gas, the outer region is bounded by the visible circular arc meniscus, and the chord joining the points where that meniscus intersects the channel walls. Within this region, the vapour partial pressure p_v satisfies the steady diffusion equation subject to the boundary condition that on the gas–liquid interface, $p_v = p_{\rm sat}$, together with the boundary condition that on the chord, p_v matches to the solution of the inner problem. Because the linearized Kelvin equation (2.2c) requires $p_v \to p_{\rm sat}$ as the film thickness becomes large, everywhere on the closed curve bounding the outer region, $p_v = p_{\rm sat}$. Throughout the outer region, p_v is therefore uniform and equal to $p_{\rm sat}$. The first conclusion of this work is that the liquid and vapour flow is completely determined by the solution of the inner problem (2.2). We have solved the boundary value problem (2.2) numerically to obtain the following results.

(a) By setting $\gamma = 0$, Derjaguin et al[1] were able to obtain an approximate solution describing evaporation from a capillary. According to our numerical solution of the complete boundary value problem (2.2), the Derjaguin solution correctly determines the evaporation rate if the length L of the gas column is large compared with the channel gap thickness $2a$; see Figure 4.2. Because the Derjaguin solution is obtained by setting $\gamma = 0$, but our condition is independent of γ, we have used our numerical solution to show that the Derjaguin approximation works because for $L/a \to \infty$, p_v is asymptotically equal to $p_{\rm sat}$ throughout the entire region in which the capillary pressure balances the disjoining pressure; see Figure 4.3. As a result, evaporation occurs only in the region in which the disjoining pressure Π determines the liquid pressure. This explains the success of the Derjaguin solution.

(b) As discussed in §1.1, existing experiments show that the diffusion–controlled meniscus of a perfectly wetting system exhibits an apparent contact angle; Θ vanishes when the system is in hydrostatic equilibrium, and is an increasing function of the potential difference $(1 - \phi)p_s$ driving evaporation. For the first time, we have posed and solved a boundary value problem

whose solution exhibits an apparent contact angle. We give the condition under which the apparent contact angle will be observed; as Figure 4.5, we give numerical results demonstrating this condition. Lastly, as equation (4.2) we give a scaling law describing the dependence of Θ on the relevant control parameters.

(c) Unlike the thermal problem, the apparent contact angle for a diffusion controlled evaporating meniscus is a function of the capillary size. To explain why, we first note that the contact angle increases with the evaporation rate, irrespective of the boundary condition driving the evaporation. In the case of a diffusion-controlled evaporating system however, the rate of evaporation is proportional to the capillary radius. This explains why the contact angle here increases with the outer length scale. In the thermal problem, the outer length scale enters the problem only through an outer boundary condition describing the bulk meniscus. Because a local analysis around the contact region does not include that outer boundary condition, the apparent contact angle for the thermal problem is independent of the outer length scale.

(d) Even though the static contact angle for a completely wetting system is zero, the stationary meniscus of a completely wetting liquid in a channel exhibits an apparent contact angle Θ that is determined chiefly by a capillary number $Ca = \mu_\ell V_s/\gamma$ based on surface tension γ, liquid viscosity μ_ℓ, and a velocity scale V_s set by evaporation. Though microphysics must be included in the boundary value problem in order to resolve the hydrodynamic singularity at the contact line, Θ is insensitive to the microphysical details. The insensitivity of Θ to the value of A has been used by Morris[36] to derive a simple formula for Θ, although for the case of an applied wall heat flux.

In the drop geometry, one will have to match a two dimensional solution near the edge of the drop to a three dimensional solution in the distant gas. This matching is extremely difficult and un-necessary since we are only interested in the dynamical processes near the contact line. For this reason, we have chosen to first study the related problem for the channel geometry, where the outer flow is largely simplified. We have analysed the simpler case of a stationary meniscus. Subsequent work accounts for boundary motion.

Appendix A

Derivation of the Governing Equations

A.1 Conditions Under Which The Simplified Kinetic Equation (2.2c) Holds

Let $\mathcal{P}(T, p_\ell^*)$ be the local co-existence pressure; i.e the vapor pressure required for liquid and vapor to co-exist at temperature T and pressure p_ℓ^*. Then by kinetic theory, $CJ^*/\lambda = (\mathcal{P} - p_v^*)$, see Cammenga[42]. Liquid thus evaporates at any point along the interface if the vapor pressure on the gas side of the interface is less than the co-existence pressure. Also, let p_o be the vapor pressure at the exit of the channel, and T_o the temperature at which liquid and vapor co-exist when both are at pressure p_o. Then following Morris[35], the kinetic equation is simplified by expanding $(\mathcal{P} - p_v^*)$ in a Taylor series about the reference state (p_o, T_o). To a first order approximation, we obtain

$$\frac{CJ^*}{\lambda} = \frac{\rho_s Q}{T_o}(T - T_o) + \frac{\rho_s}{\rho_\ell}(p_\ell^* - p_o) - (p_v^* - p_o) \tag{A.1}$$

where ρ_ℓ is the liquid density, Q the latent heat of vaporization, C the speed of sound in the gas, $\lambda = \sqrt{2\sigma/\pi}$ a kinetic constant, σ the specific heat ratio, and ρ_s the saturation vapour density at temperature T_o. In the thicker portions of the meniscus, i.e on the scale of the channel gap thickness, diffusion is rate limiting; as a result, the term on the left of (A.1) vanishes far from the contact line. Hence, we apply the condition that $J \to 0$ at infinity to obtain

$$0 = \frac{\rho_s Q}{T_o}(T_w - T_o) + \frac{\rho_s}{\rho_\ell}(p_b - p_o) - (p_s - p_o) \tag{A.2}$$

where far from the wall, the interface temperature is assumed to be equal to the wall temperature; evaporative cooling is therefore taken as negligible at infinity. p_s is the saturation pressure at temperature T_o. Equation A.2 gives T_o as a function of the boundary values p_b, p_s, p_o, and T_w which are all given as part of the solution. By subtracting equation A.2 from A.1, we obtain

$$\frac{CJ^*}{\lambda} = \frac{\rho_s Q}{T_o}(T - T_w) + \frac{\rho_s}{\rho_\ell}(p_\ell^* - p_b) - (p_v^* - p_s) \tag{A.3}$$

In equation A.3, T_o can be replaced by T_w because $|T_w - T_o| << T_o$ in applications. We have therefore eliminate T_o and p_o in favour of known boundary values. Because there is no build up of mass at the interface, specie mass balance there requires that the rate of transfer of molecules across the interface be equal to the diffusion flux evaluated at the interface. Specifically

$$-\Lambda \frac{\partial p_v^*}{\partial n} = \frac{\rho_s Q}{T_w}(T - T_w) + \frac{\rho_s}{\rho_\ell}(p_\ell^* - p_b) - (p_v^* - p_s) \tag{A.4}$$

where $\Lambda = CD_v/\lambda R_v T_w$ is the mean free path of the vapor molecules in the gas. The mixed boundary condition (A.4) couples the dynamical processes in the surrounding gas to those in the liquid phase. This coupling of the different physics make direct analysis difficult. We therefore make the following simplifying assumptions: (i) The continuum approximation holds within the surrounding gas; as a result, liquid and vapor at the interface are in local thermodynamic equilibrium. (ii) The system is effectively isothermal; though evaporation induces liquid temperature differences, they are kinetically negligible for the slow evaporation processes considered here.

Given (i) and (ii), equation A.4 simplifies to

$$p_v^* = p_s + \frac{\rho_s}{\rho}(p_\ell^* - p_b) \tag{A.5}$$

A.2 Conditions for Isothermal Evaporation

The latent heat consumption caused by evaporation at the interface induces temperature gradients within the drop, substrate, and surrounding gas. One can estimate the order of magnitude for temperature differences within the drop by making use of the energy balance $\kappa \nabla T \cdot n_1 = QJ^*$ at the interface, where κ is the liquid thermal conductivity, n_1 the unit normal to the interface with the other parameters defined above. The energy balance states that all heat conducted from the wall to the interface is absorbed as latent heat. Because there is no build up of mass at the interface, the evaporative flux term J is estimated using Fick's law $J = D_v \nabla c \cdot n_2$, where n_2 is the unit normal at the interface into the gas and $c = p_v^*/R_v T_w$. Eliminating J between the two equations, Fick's law and energy balance, we find that at the interface

$$\kappa \frac{\partial T}{\partial n_1} = \frac{QD_v}{R_v T_w} \frac{\partial p_v^*}{\partial n_2} \tag{A.6}$$

To a first approximation, the vapour flow occurs in a half-space and so has just one length scale δ/Θ, where δ is a characteristic film thickness. Near the contact line, where temperature differences across the drop are highest, the liquid flow occurs in a wedge of contact angle Θ, and so has two length scales δ/Θ and δ. Then, according to equation A.6, we estimate that

$$\Delta T \sim \Theta \frac{QD_v}{\kappa R_v T_w} p_s (1 - \phi) \tag{A.7}$$

where p_s is the saturation vapour pressure, ϕ the relative humidity in the distant gas, and ΔT the characteristic temperature difference across the drop. According to equation A.4, temperature differences within the drop are kinetically negligible if the first term on the right is negligibly small as compared to the third term; i.e if $\rho_s Q \Delta T / T_w << p_s(1 - \phi)$, which translates to

$$\epsilon = \frac{\rho_s Q^2 D_v \Theta}{\kappa R_v T_w^2} << 1 \tag{A.8}$$

Both ϵ and ΔT depend on the drop size through Θ. The parameter ϵ is given in Sultan et al (2005, row 7, table 2)[11] as the ratio of a thermal expansion

number to a kinetic Peclet number; in their notation $\epsilon = \chi/Pe_k$.

In table A.1, we give some estimates for the parameters. Values of Θ for the first two rows are taken from Cachile et al[14]; the last row from Deegan et al[19]. The relative humidity $\phi = 0$ for the organic liquids and $\phi = 0.4$ for water. The table shows that temperature gradients, and hence Marangoni

Liquid	$\Theta(rad)$	$\Delta T(K)$	ϵ
Octane[14]	0.015	0.10	0.007
Heptane[14]	0.030	0.23	0.011
Water[19]	0.26	15.62	1.56

Table A.1: Estimates for ΔT and ϵ

flows, become increasingly significant as the drop thickness increases; i.e for drops with large Θ. This does not mean that heat conduction becomes the controlling mechanism because for that to happen, the drop size must be small compared with the mean free path Λ of the vapour in the gas.

A.3 Derivation of Equation (2.2a)

To simplify the problem, we assume that transport of the vapour molecules in the gas is by axial diffusion only; though there are concentration gradients in the radial direction, they are negligibly small in the limit $a/L \to 0$. Balancing mass on the differential control volume in figure 2.1a requires that

$$\dot{m}_x + \dot{m}_g - \dot{m}_{x+dx} = \frac{d}{dt} m_{sys} \tag{A.9}$$

Where $\dot{m}_x$ is the rate at which mass is entering the control volume, $\dot{m}_g$ the rate at which mass is generated within the control volume, $\dot{m}_{x+dx}$ the rate at which mass is leaving the control volume, and m_{sys} the total mass within the control volume at any given instant. These quantities are given as

$$\dot{m}_x = \frac{D_v p}{R_v T_w} A_c(x) \frac{d}{dx} \ln\left(1 - \frac{p_v}{p}\right) \tag{A.10a}$$

$$\dot{m}_g = J(x) dA_s \tag{A.10b}$$

$$\dot{m}_{x+dx} = \dot{m}_x + \frac{d\dot{m}_x}{dx} dx \tag{A.10c}$$

Where $A_c(x)$ is the cross-sectional area of the channel, dA_s the surface area of the differential element, $p_v(x)$ the vapour pressure, $J(x)$ the evaporative mass flux normal to the interface, p the total gas pressure, D_v the binary diffusion coefficient, R_v the specific gas constant, and T_w the wall temperature. Equation A.10a expresses Fick's first law; it assumes that the medium into which evaporation occurs is stationary, and that the gas mixture is ideal. Taylor expanding equation A.10a gives us A.10c. For a channel made up of two parallel plates, $A_c(x) = a - h(x)$ and $dA_s = dx$ per unit depth of channel. Due to symmetry, we have considered only the lower half of the channel. Under steady state conditions, equations A.9 and A.10 gives

$$J = \frac{D_v p}{R_v T_w} \frac{d}{dx} \left[(a - h) \frac{d}{dx} \ln\left(1 - \frac{p_v}{p}\right) \right] \tag{A.11}$$

Using lubrication theory, the mass flow rate in the thin quasi-parallel liquid film is related to the local evaporative mass flux J by

$$\frac{d}{dx} \left[\frac{h^3}{3\nu} \frac{dp_\ell}{dx} \right] = J \tag{A.12}$$

Equation (A.12) neglects shear stress at the interface. We now eliminate J between equations (A.11) and (A.12); then integrate once to show that

$$\frac{h^3}{3\nu} \frac{dp_\ell}{dx} - \frac{D_v p}{R_v T_w} (a - h) \frac{d}{dx} \ln\left(1 - \frac{p_v}{p}\right) = -\dot{m} \tag{A.13}$$

For $p_v/p \to 0$ and for $h << a$, equation (A.13) reduces to (2.2a).

Appendix B

Numerical Analysis

This chapter describes the use of the general-purpose code d02tkf, together with its associated routines d02tvf, d02txf, d02tyf, and d02tzf; all obtained from the NAG numerical library. The code is based on modified versions of the codes COLSYS and COLNE, Ascher et al[44] and Ascher and Bader[45], and is capable of solving mixed-order systems of ordinary differential equations in boundary value problems. First, d02tvf is called to specify the initial mesh, error requirements, and other details. Then d02tkf is called to solve the boundary value problem in question. After successful computation, d02tzf is used to examine details about the final mesh. Finally, d02tyf is used to approximate the solution anywhere on the solution domain using polynomial interpolation. In case of a continuation, as it is with this problem, d02txf allows the solution values computed in the previous call to d02tkf to be used as an initial guess to the solution in the next call to d02tkf. This avoids the overhead of a complete initialisation when the setup routine d02tvf is called.

Consider a mixed-order system of n nonlinear ordinary differential equations of orders $1 \leq k_1 \leq k_2 \leq ... \leq k_n \leq 4$ over the interval $a \leq x \leq b$,

$$y_i^{(k_i)} = f_i\left(x; \mathbf{z}(\mathbf{y})\right), \qquad i = 1, 2, ...n \tag{B.1}$$

where $\mathbf{y} = (y_1, y_2, ...y_n)$ is the solution vector and $y_j^{(k)}$ the k^{th} derivative of the j^{th} solution component. Hence, $y_j^{(0)} = y_j$ and $\mathbf{z}(\mathbf{y})$ is the vector of unknowns, $\mathbf{z}(\mathbf{y}) = \left(x, y_1, y_1^{(1)}..., y_1^{(k_1-1)}, y_2, y_2^{(1)}..., y_2^{(k_2-1)}, ...y_n, y_n^{(1)}..., y_n^{(k_n-1)}\right)$, that would result from converting (B.1) into a system of first order equations. The sys-

tem is subjected to p nonlinear boundary conditions at a and q nonlinear boundary conditions at b, where $p+q=\sum_{l=1}^{n} k_l$. The left and right nonlinear boundary conditions at a and b are therefore defined respectively as,

$$g_i\left(a;\mathbf{z}(\mathbf{y})\right)=0, \qquad i=1,2,.....p \tag{B.2a}$$
$$g_j\left(b;\mathbf{z}(\mathbf{y})\right)=0, \qquad j=1,2,.....q \tag{B.2b}$$

The ode solver d02tkf, and its associated routines, uses the method of spline collocation to solve equations (B.1) and (B.2). Approximate solutions are computed on a sequence of automatically selected meshes until a user specified set of tolerances for the solution components $\mathbf{y}$ are satisfied. A damped Newton method is used for the nonlinear iteration. The user must supply a set of subroutines for evaluating the functions f_i given x and $\mathbf{z}(\mathbf{y})$, the partial derivative of f_i with respect to $\mathbf{z}(\mathbf{y})$, the partial derivative of g_i with respect to $\mathbf{z}(\mathbf{y})$, boundary conditions, and initial approximations to $\mathbf{z}(\mathbf{y})$.

B.1 Fortran Program Listing

To solve problem (2.7) using the ode solver d02tkf described above, the equations are first expressed in the form of the mixed order system (B.1). Because the slope unit $\Theta_s << 1$, the problem domain is infinite. This example uses continuation in the parameters α and Θ_s. The equations are first mapped onto the interval $[-\chi,1)$ using the transformation $\hat{x}=x\Theta_s$ to yield,

$$p_\ell''=-3h^2h'p_\ell'\left(h^3+3\beta\right)^{-1}, \tag{B.3a}$$
$$h''=\left(1-p_\ell-h^{-3}\right)\lambda^2. \tag{B.3b}$$

For convenience, we have replaced Θ_s with λ^{-1}. The system of two equations, each of second order, are subject to the following boundary conditions

$$p_\ell(-\chi)+\alpha=0, \qquad h(-\chi)-h_o=0, \tag{B.4c,d}$$
$$p_\ell(1)=0, \qquad h'(1)-\lambda^2=0 \tag{B.4e,f}$$

where h_o is the film thickness at the channel mouth; $h_o^3 = (1+\alpha)^{-1}$. Superscripts h' represents differentiation with respect to $\hat{x}$. The numerical scheme first obtain solutions for the simple case $\alpha = 0$ and $\lambda > 1$ using the initial approximations $p = 0$ and $h = 1$. The obtained solutions are then used as initial guesses in the solution for $\alpha = \alpha + \Delta\alpha$ and $\lambda = \lambda + \Delta\lambda$. The process is repeated until we obtain solutions for the values α and λ that we desire.

B.1.1 Main Program

```
!*****************************************************************
! odesolver.f90
!
! FUNCTIONS:
! odesolver - Entry point of console application.
!
!
! PROGRAM: odesolver
!
! PURPOSE: solves a general two-point boundary value problem for a
! non-linear mixed order system of ordinary differential equations.
!
!*****************************************************************

    program odesolver

    ! use statements

    use nag_library, only : d02tkf, d02tvf, d02txf, d02tyf, d02tzf

    use odesolver_mod, only : λ, ffun, fjac, gafun, gajac, gbfun, gbjac, &
                              guess, m1, m2, mmax, nag_wp, neq, nin, &
                              nout, nrbc, zero, one, α, two, beta, six, N2, &
                              LB, RB, nlbc, chi

    ! implicit none statement

    implicit none
```

```
! local scalars
real (kind=nag_wp) :: dx, λ_init, ermx, α_init, xx
integer :: i, iermx, ifail, ijermx, j, nmesh, &
           liwork, lrwork, mxmesh, ncol, ncont

! local arrays
real (kind=nag_wp), allocatable :: mesh(:), rwork(:)
real (kind=nag_wp) :: tol(neq), y(neq,0:mmax-1)
integer, allocatable :: ipmesh(:), iwork(:)
integer :: m(neq)

!************************************************
! Begin user-supply parameter values
!************************************************

! Parameters and boundary locations
beta = 0.1_nag_wp     ! See equation 2.8
chi = 5.0_nag_wp      ! See equation 2.8
LB = - chi     ! Left Boundary
RB = one     ! Right Boundary

! executable statements
write (nout,*) 'D02TXF: Research Program in Progress'
write (nout,*) '*********************************'
ncol = 6     ! Number of collocation points;
           ! Constraint:     mmax ≤ ncol ≤ 7
nmesh = 5.0_nag_wp + two*chi     ! Number of initial mesh points,
           ! Constraint:     6 < nmesh < mxmesh/2
mxmesh = 10000     ! Maximum number of mesh points allowed,
           ! Constraint:     mxmesh ≥ 2(nmesh − 1)
tol(1:neq) = (0.0000001,0.0000001)  ! tolerance for each solution component
liwork = mxmesh*(11*neq+6)     ! do not modify
lrwork = mxmesh*(109*neq**2+78*neq+7)     ! do not modify
allocate (mesh(mxmesh),rwork(lrwork),ipmesh(mxmesh),iwork(liwork))

! Enter initial parameters
λ_init = 30.0_nag_wp     ! Initial value of λ
α_init = zero     ! initial value of α
```

```
! Initialize data
λ = λ_init
α = α_init
m(1) = m1     ! order of the first differential equation
m(2) = m2     ! order of the second differential equation
dx = (RB-LB)/real(nmesh-1,kind=nag_wp)     ! step size
mesh(1) = LB     ! left boundary point

!**********************************************************************
! End user-supply parameter values:
!**********************************************************************

do i = 2, nmesh-1
    mesh(i) = mesh(i-1) + dx     ! initial mesh points
end do

mesh(nmesh) = RB     ! right boundary point
ipmesh(1) = 1 ! a constraint; fixes the left boundary point
ipmesh(2:nmesh-1) = 2 ! 1 for fixed internal mesh points; 2 for otherwise
ipmesh(nmesh) = 1 ! a constraint; fixes the right boundary point

! initial integrator for given problem
ifail = 0     ! Error indicator
call d02tvf(neq,m,nlbc,nrbc,ncol,tol,mxmesh,nmesh,mesh,ipmesh,rwork, &
            lrwork,iwork,liwork,ifail)

ncont = 2000     ! number of continuation steps in λ and α
cont: do j = 1, ncont
! solve problem
ifail = -1
call d02tkf(ffun,fjac,gafun,gbfun,gajac,gbjac,guess,rwork,iwork,ifail)
if (ifail/=0) exit cont
! extract mesh
ifail = 0
call d02tzf(mxmesh,nmesh,mesh,ipmesh,ermx,iermx,ijermx,rwork,iwork,ifail)

! select mesh for continuation and update continuation parameters
```

```
if (j<ncont) then
λ = λ + 100.0_nag_wp/real(ncont-1,kind=nag_wp)
α = α + one
nmesh = (nmesh+1)/2
ifail = 0
call d02txf(mxmesh,nmesh,mesh,ipmesh,rwork,iwork,ifail)
end if
end do cont

write (nout,99997) tol(1), λ, α
! print mesh and error statistics
write (nout,99996) nmesh, ermx, iermx, ijermx
! print solution components on mesh
write (nout,99999)
dx = (RB-LB)/real(N2-1,kind=nag_wp) ! Evaluate at N2 uniform grid points
xx = LB      ! Begin evaluation at left boundary
open (2, file='beta04.txt')     ! open file
do i = 1, N2
ifail = 0
call d02tyf(xx,y,neq,mmax,rwork,iwork,ifail)
write (2,99998) xx, y(1,0), y(2,0) ! write to file
xx = min(one,xx + dx)
end do
close (2, status='keep') ! close file; includes last solution only

99999 format (//4X,'x',16X,'p',16X,'h')
99998 format (1X,F16.8,2(1X,F20.8))
99997 format (//'tolerance = ',E8.1,' λ =',F12.3,' α =',F12.3)
99996 format (/'used a mesh of ',I4,'points'/'maximum error = ',E10.2, &
                ' in interval ',I4,' for component ',I4)

    end program odesolver
```

B.1.2 The Module

```
!***********************************************
! Parameters and user-defined subroutines: This module
```

```
! contains seven user-defined subroutines, namely; ffun,
! fjac, gafun, gbfun, gajac, gbjac, and guess
!************************************************

    module odesolver_mod

    ! use statements

    use nag_library, only : nag_wp

    implicit none

real (kind=nag_wp), parameter :: zero = 0.0_nag_wp
real (kind=nag_wp), parameter :: one = 1.0_nag_wp
real (kind=nag_wp), parameter :: two = 2.0_nag_wp
real (kind=nag_wp), parameter :: three = 3.0_nag_wp
real (kind=nag_wp), parameter :: four = 4.0_nag_wp
real (kind=nag_wp), parameter :: six = 6.0_nag_wp
real (kind=nag_wp), parameter :: nine = 9.0_nag_wp
integer, parameter :: m1 = 2, m2 = 2, mmax = 2, neq = 2, N2 = 10000, &
                      nin = 5, nlbc = 2, nout = 6, nrbc = 2
real (kind=nag_wp) :: λ, α, beta, LB, RB, chi

! *****************************************************
! Parameter Definitions
! *****************************************************
! m1 = order of first ode (equation B.3a)
! m2 = order of second ode (equation B.3b)
! nlbc = number of left boundary conditions
! nrbc = number of right bcs
! neq = number of differential equations to be solved
! λ, chi, α, beta : parameters in the boundary value problem
! mmax = maximum order of the differential equations
! N2 = Number of interpolation points
! *****************************************************

    contains       ! user-defined subroutines
```

```
! ************************************************************
! subroutine ffun: Lists the system of neq
! differential equations to be solved
! ************************************************************

! y(m,n) = the nth derivative of the mth component

subroutine ffun(x,y,neq,m,f)

    implicit none

real (kind=nag_wp), intent (in) :: x ! the independent variable
integer, intent (in) :: neq ! number of differential equations to be solved
real (kind=nag_wp), intent (out) :: f(neq)
real (kind=nag_wp), intent (in) :: y(neq,0:*)
integer, intent (in) :: m(neq)
real (kind=nag_wp) :: t1, y21, y20, y11
y20 = y(2,0) ! = h
y21 = y(2,1) ! = h'
y11 = y(1,1) ! = p'
t1 = three*beta + y20*y20*y20
f(1) = - three*y20*y20*y21*y11/t1      ! equation B.3a
f(2) = λ*λ*(one-y(1,0)-(one/(y20*y20*y20)))      ! equation B.3b
return
end subroutine ffun

! ************************************************************
! subroutine fjac: Jacobian for the system of equations
! ************************************************************

! f(1) = p''(p,p',h,h') and f(2) = h''(p,p',h,h'). Then
! dfdy(i,j,k) = df(i)dy(j,k), where y(j,k) = [p,p',h,h']
! i = 1,2...neq
! dfdy(i, j, k) = ∂f_i/∂y_j^(k)

subroutine fjac(x,y,neq,m,dfdy)

    implicit none
```

```
real (kind=nag_wp), intent (in) :: x
integer, intent (in) :: neq
real (kind=nag_wp), intent (inout) :: dfdy(neq,neq,0:*)
real (kind=nag_wp), intent (in) :: y(neq,0:*)
integer, intent (in) :: m(neq)
real (kind=nag_wp) :: t1, y21, y20, y11
y20 = y(2,0) ! = h
y21 = y(2,1) ! = h'
y11 = y(1,1) ! = p'
t1 = three*beta + y20*y20*y20
dfdy(1,2,1) = - (three*y20*y20*y11)/t1
dfdy(1,1,1) = - (three*y20*y20*y21)/t1
dfdy(1,2,0) = (nine*y21*y11*(y20**four))/(t1*t1) - six*y21*y11*y20/t1
dfdy(2,2,0) = three*λ*λ/(y20*y20*y20*y20)
dfdy(2,1,0) = - λ*λ
return
end subroutine fjac

! ***********************************************************************
! Subroutine gafun: Evaluates the boundary conditions at the left
! hand end of the solution domain. First entry in ya(a1,a2) gives the
! solution component; second entry gives the order of the derivative.
! For example ya(1,0) = p; ya(1,1) = p'; ya(2,0) = h; ya(2,1) = h'.
!***********************************************************************

subroutine gafun(ya,neq,m,nlbc,ga)

    implicit none

integer, intent (in) :: neq, nlbc
real (kind=nag_wp), intent (out) :: ga(nlbc)
real (kind=nag_wp), intent (in) :: ya(neq,0:*)
integer, intent (in) :: m(neq)
ga(1) = ya(1,0) + α ! p(-1) = -α
ga(2) = ya(2,0) - (one/(one+α))**(one/three) ! h(-1) = (1/(1+α))**(1/3)
return
end subroutine gafun
```

```
! ******************************************************
! Subroutine gbfun: Evaluates the boundary conditions at the right
! hand end of the solution domain. Entries as described in gafun
!******************************************************

subroutine gbfun(yb,neq,m,nrbc,gb)

    implicit none

integer, intent (in) :: neq, nrbc
real (kind=nag_wp), intent (out) :: gb(nrbc)
real (kind=nag_wp), intent (in) :: yb(neq,0:*)
integer, intent (in) :: m(neq)
gb(1) = yb(1,0) ! p(1) = 0
gb(2) = yb(2,1) - λ*λ*RB      ! h'(1) = λ*λ*x
return
end subroutine gbfun

! ******************************************************
! Subroutine gajac: Evaluates the Jacobian at the left hand
! end of the solution domain. Entries as described in fjac
!******************************************************

subroutine gajac(ya,neq,m,nlbc,dgady)

    implicit none

integer, intent (in) :: neq, nlbc
real (kind=nag_wp), intent (inout) :: dgady(nlbc,neq,0:*)
real (kind=nag_wp), intent (in) :: ya(neq,0:*)
integer, intent (in) :: m(neq)
dgady(1,1,0) = one
dgady(2,2,0) = one
return
end subroutine gajac

! ******************************************************
```

```
! Subroutine gbjac: Evaluates the Jacobian at the right hand
! end of the solution domain. Entries as described in fjac
!*******************************************************

subroutine gbjac(yb,neq,m,nrbc,dgbdy)

    implicit none

integer, intent (in) :: neq, nrbc
real (kind=nag_wp), intent (inout) :: dgbdy(nrbc,neq,0:*)
real (kind=nag_wp), intent (in) :: yb(neq,0:*)
integer, intent (in) :: m(neq)
dgbdy(1,1,0) = one
dgbdy(2,2,1) = one
return
end subroutine gbjac

! *****************************************
! Subroutine guess: user-supplied initial guesses for
! the solution components, h and p_ℓ
! *****************************************

subroutine guess(x,neq,m,y,dym)

    implicit none

real (kind=nag_wp), intent (in) :: x
integer, intent (in) :: neq
real (kind=nag_wp), intent (out) :: dym(neq)
real (kind=nag_wp), intent (inout) :: y(neq,0:*)
integer, intent (in) :: m(neq)
y(1,0) = zero ! p; example: y(1,0) = x**2 + one
y(1,1) = zero ! p'
y(2,0) = one ! h
y(2,1) = zero ! h'
dym(1) = zero ! p''
dym(2) = zero ! h''
return
```

```
end subroutine guess

    end module odesolver_mod
```

References

1. Derjaguin B.V., Nerpin S.V., Churayev N.V. *'Effect of film transfer upon evaporation of liquids from capillaries.'* Bulletin Rilem, **29**, (1965), pp. 93-98.

2. Morse H.W. *'Evaporation from the surface of a solid sphere.'* Proc. Amer. Acad. Sci., **45**, (1910), pp. 363-367.

3. Langmuir I. *'The Evaporation of Small Spheres.'* Phys. Rev., **12**, (1918), pp. 368-370.

4. Soltman D. and Subramanian V. *'Inkjet Printed Line Morphologies and Temperature Control of the Coffee Ring Effect.'* Langmuir, **24**, (2008), pp. 2224-2231.

5. Jing J., Reed J., Huang J., Hu X., Clarke V., Edington J., Housman D., Anantharaman T., Huff E., Mishra B., Porter B., Shenker A., Wolfson E., Hiort C., Kantor R., Aston C., Schwarzt D. *'Automated High Resolution Optical Mapping using Arrayed, Fluid-Fixed DNA Molecules .'* Proc. Natl. Acad. Sci. USA, **95**, isuue 14, (1998), pp. 8046-8051.

6. Ondarcuhu T. and Joachim C. *'Drawing a Single Nanofibre Over Hundreds on Microns.'* Europhys. Lett., **42**, issue 2, (1998), pp. 215-220.

7. Zhang D., Xie Y., Mrozek M.F., Ortiz C., Davisson V.J., Ben-Amotz D. *'Raman Detection of Proteomic Analytes.'* Anal. Chem., **21**, issue 75, (2003), pp. 5703-5709.

8. Burelbach J.P., Bankoff S.G., Davis S.H. *'Nonlinear Stability of Evaporating/Condensing Liquid Films.'* J. Fluid Mech., **195**, (1988), pp. 463-494.

9. Dondlinger M., Margerit J., Dauby P.C. *'Weakly Nonlinear Study of Marangoni instabilities in an Evaporating Liquid Layer.'* J. Colloid Interface Sci., **283**, (2005), pp. 522-532.

10. Stephen W. *'Role of the Species Momentum Equation in the Analysis of the Stefan Diffusion Tube.'* Ind. Eng. Chem. Res., **30**, (1991), pp. 978-983.

11. Sultan E., Boudaoud A., Amer M.B.*'Evaporation of a thin film: diffusion of the vapour and marangoni instabilities.'* J. Fluid Mech., **543**, (2005), pp. 183-202.

12. Cazabat A-M. and Guena G., *'Evaporation of Macroscopic Sessile Droplets.'* Soft Matter, **6**, (2010), pp. 2591-2612.

13. Guena G., Poulard C., Voue M., De Coninck D., Cazabat A-M. *'Evaporation of Sessile Liquid Droplets.'* Colloids and Surfaces A: Physicochem. Eng. Aspects, **291**, (2006), pp. 191-196.

14. Cachile M., Benichou O., Cazabat A-M, *'Evaporating Droplets of Completely Wetting Liquids.'* Langmuir, **18**, (2002), pp. 7985-7990

15. Poulard C., Guena G., Cazabat A-M, Boudaoud A., Amer B.M. *'Rescaling the Dynamics of Evaporating Drops.'* Langmuir, **21**, (2005), pp. 8226-8233

16. Benichou O., Cachile M., Cazabat A-M., Poulard C., Valignat M.P., Vandenbrouck F., Van Effenterre D. *'Thin Films in Wetting and Spreading.'* Adv. Colloid and Interface science, **101-102**, (2003), pp. 381-398

17. Guena G., Poulard C., Cazabat A-M, *'The Leading Edge of Evaporating Droplets.'* Colloid and Interface science, **312**, (2007), pp. 164-171

18. Deegan R.D, Bakajin O., Dupont T.F., Huber G., Nagel S.R., Witten T.A. *'Capillary Flow as the Cause of Ring Stains From Dried Liquid Droplets.'* Nature, **389**, (1997), pp. 827-829.

19. Deegan R.D., Bakajin O., Dupont T.F., Huber G., Nagel S.R., and Witten T.A. *'Contact Line Deposits in an Evaporating Drop.'* Phys. Rev. E, **62**, (2000), pp. 756-765, No 1.

20. Deegan Robert *'Pattern Formation in Drying Drops.'* Phys. Rev. E, **61**, (2000), pp. 475-485, No 1.

21. Picknett R.G. and Bexon R. *'The Evaporation of Sessile or Pendant Drops in Still Air.'* J. Colloid Interface Sci., **61**, (1977), pp. 336-350, No 2.

22. Yuri Popov *'Evaporative Deposition Pattern: Spatial Dimensions of the Deposit.'* Phys. Rev. E, **71**, (2005), 036313.

23. Hu H. and Larson R.G. *'Evaporation of a Sessile Droplet on a Substrate.'* J. Phys. Chem. B, **106**, (2002), pp. 1334-1344.

24. Hu H. and Larson R.G. *'Analysis of the Effects of Marangoni Stresses on the Microflow in an Evaporating Sessile Droplet.'* Langmuir, **21**, (2005), pp. 3972-3980.

25. Hu H. and Larson R.G. *'Analysis of the Microfluid Flow in an Evaporating Sessile Droplet.'* Langmuir, **21**, (2005), pp. 3963-3971.

26. DasGupta Sunando et al., *'Use of the Augmented Young-Laplace Equation to Model Equilibrium and Evaporating Extended Meniscus.'* J. Colloid Int. Sci., **157**, (1993), pp. 332-342.

27. DasGupta S., Kim I.Y., Wayner P.C. *'Use of the kelvin-Clapeyron Equation to Model an Evaporating Curved Microfilm.'* J. Heat Transfer, **116**, (1994), pp. 1007-1015.

28. Kim Y. and P.C Wayner, *'Shape of an Evaporating Completely Wetting Extended Meniscus.'* J. Thermophysics and Heat Transfer, **10**, Issue 2, (1996), pp. 320-325.

29. Schonberg J.A., DasGupta S., Wayner P.C. *'An Augmented Young-Laplace Model of an Evaporating Meniscus in a Microchannel with High Heat Flux.'* Experimental Thermal and Fluid science., **10**, (1995), pp. 163-170

30. Truong J.G and Wayner P.C., *'Effect of Capillary and Van der Waals Dispersion Forces on the Equilibrium Profile of a Wetting Liquid: Theory and Experiment.'* J. Chem. Phys., **87**, (1987), pp. 4180-4188

31. Schonberg J.A. and Wayner P.C. *'Analytical Solution for the Integral Contact Line Evaporative Heat Sink .'* J. Thermophys. Heat Transfer, **6**(1), (1992), pp. 128-134.

32. Steven Moosman and G.M. Homsy *'Evaporating Menisci of Wetting Fluids.'* J. Colloid Int. Sci., **73**, No 1, (1980), pp. 212-223

33. Renk F., Wayner P.C., and Homsy G.M. *'On the transition Between a Wetting Film and a Capillary Meniscus.'* J. Colloid Int. Sci., **67**, No 3, (1978), pp. 408-414

34. Stephan P.C., and Busse C.A. *'Analysis of the heat transfer coefficient of grooved heat pipe evaporator walls.'* Int. J. Heat Mass Transfer, **35**, No2, (1992), pp. 383-391.

35. Morris S.J.S., *'A phenomenological model for the contact region of an evaporating meniscus on a superheated slab.'* J. Fluid Mech., **411**, (2000), pp. 59-89.

36. Morris S.J.S., *'Contact angles for evaporating liquids predicted and compared with existing experiments.'* J. Fluid Mech., **432**, (2001), pp. 1-30.

37. Morris S.J.S., *'The evaporating meniscus in a channel.'* J. Fluid Mech., **494**, (2003), pp. 297-317

38. Oron A., Davis S.H., Bankoff S.G. *'Long-Scale Evolution of Thin Liquid Films.'* rev. Mod. Phys., **69**, (1997), pp. 931-980.

39. Hervet H. and de Gennes P.G. *'The Dynamics of Wetting: Precursor Films in the Wetting of Dry Solids.'* C.R. Acad. Sci. Paris,**299**, Series II, no 9, (1984), pp. 499-503.

40. Joanny J.F. *'Dynamics of wetting: Interface profile of a spreading liquid.'* J. Theor. Appl. Mech., **23**, (1986), pp. 249-271.

41. Jensen O.E. and Grotberg J.B, *'The Spreading of a Heat or Soluble Surfactant Along a Thin Liquid Film.'* Phys. Fluids A, **5**, (1997), pp. 58-68.

42. Cammenga Heiko K., *'Evaporation mechanisms of liquids.'* Current topics in materials science, **5**, (1980), Chapter four (Equation 11).

43. Bird R. B., Stewart E. W., Lightfoot N. E. *'Transport Phenomena.'* Wiley, New York, (2006), Chapter 18.

44. Ascher U.M., Christiansen J., Russel R.D., *'A collocation solver for mixed order systems of boundary value problems.'* Math. Comput., **33**, (1979), pp. 659-679.

45. Ascher U. M and Bader G., *'A new basis implimentation for a mixed order boundary value ODE solver.'* SIAM J. Sci. Stat. Comput., **8**, (1987), pp. 483-500.

46. Jackson J.D. *'Classical Electrodynamics.'* Wiley, New York, (1975), p.77 2nd ed.